Communications on Applied Mathematics and Computation (2024) 6:1924–1953
https://doi.org/10.1007/s42967-023-00348-9

ORIGINAL PAPER

# Revisting High-Resolution Schemes with van Albada Slope Limiter

**Jingcheng Lu**[1,2] · **Eitan Tadmor**[3]

*To Rémi Abgrall with friendship and appreciation.*

Received: 6 April 2023 / Revised: 7 August 2023 / Accepted: 29 October 2023 /
Published online: 19 February 2024


**Abstract**
Slope limiters play an essential role in maintaining the non-oscillatory behavior of high-resolution methods for nonlinear conservation laws. The family of minmod limiters serves as the prototype example. Here, we revisit the question of non-oscillatory behavior of high-resolution central schemes in terms of the slope limiter proposed by van Albada et al. (Astron Astrophys 108: 76–84, 1982). The van Albada (vA) limiter is smoother near extrema, and consequently, in many cases, it outperforms the results obtained using the standard minmod limiter. In particular, we prove that the vA limiter ensures the one-dimensional Total-Variation Diminishing (TVD) stability and demonstrate that it yields noticeable improvement in computation of one- and two-dimensional systems.

**Keywords** High resolution · Limiters · Total-Variation Diminishing (TVD) stability · Central schemes

**Mathematics Subject Classification** 35L65 · 65M10

## 1 Introduction

We revisit the class of high-resolution, non-oscillatory schemes for the approximate solution of nonlinear conservation laws. This class of schemes went through an intense period of development during the 1980s and 1990s. By high resolution, we refer to the class of

✉ Eitan Tadmor
tadmor@umd.edu

Jingcheng Lu
lu000688@umn.edu

[1] Department of Mathematics, University of Maryland, College Park, MD, USA

[2] School of Mathematics, University of Minnesota, Minneapolis, MN, USA

[3] Department of Mathematics and Institute for Physical Sciences and Technology, University of Maryland, College Park, MD, USA

schemes which are formally second-order or higher-order methods at all computational cells, except perhaps for finitely many critical cells, thus breaking the first-order accuracy barrier of Godunov for monotone schemes [16]. By non-oscillatory, we refer to classes of schemes which satisfy certain types of stability bounds—weaker than monotonicity yet strong enough to exclude spurious oscillations. In this context, we mention the canonical example of Total-Variation Diminishing (TVD) schemes of Harten [5, 14, 39, 40, 49]. Other classes of non-oscillatory stable schemes followed, including finite-volume, finite-element, Discontinuous Galerkin (DG), and spectral schemes; as examples, we mention the Total-Variation Bounded (TVB) schemes [20, 34, 43, 52, 57], the One-Sided Lip Condition (OSLC) bounded E-schemes [37, 50], and entropy stable schemes [8, 54]. We also mention the notable class of Essentially Non-Oscillatory (ENO) and Weighted ENO (WENO) schemes [15, 32, 45, 46] and their sign property stability bound [8–10].

In this paper, we focus on second-order Godunov-type methods. The key step of such methods is the second-order accurate reconstruction. To fix our notations, we consider the one-dimensional, piece-wise constant scalar numerical solution at time level $t^n := n\Delta t$, which is realized in terms of its cell averages $\{\bar{u}^n_\alpha = \bar{u}(x_\alpha, t^n)\}$ over equi-spaced mesh $\{x_\alpha \colon x_\alpha = \alpha\Delta x\}$

$$u^n = \sum_j \bar{u}^n_j \mathbb{1}_{\left[x_{j-\frac{1}{2}}, x_{j+\frac{1}{2}}\right]}, \qquad \bar{u}(x_j, t^n) := \frac{1}{\Delta x}\int_{x_{j-\frac{1}{2}}}^{x_{j+\frac{1}{2}}} u(x, t^n)\mathrm{d}x, \qquad j \in \mathbb{Z}.$$

The key ingredient of Godunov-type schemes is a piece-wise linear reconstruction, $u^{\Delta x}(x, t^n) \approx u(x, t^n)$, which conserves the underlying cell averages, $\frac{1}{\Delta x}\int_{x_{j-\frac{1}{2}}}^{x_{j+\frac{1}{2}}} u^{\Delta x}(x, t^n)\mathrm{d}x = \bar{u}^n_j$. Thus, $u^{\Delta x}(x, t^n)$ takes the form

$$u^{\Delta x}(x, t^n) = \sum_j p^n_j(x)\mathbb{1}_{\left[x_{j-\frac{1}{2}}, x_{j+\frac{1}{2}}\right]}, \qquad p^n_j(x) = \bar{u}^n_j + \frac{u'_j}{\Delta x}(x - x_j). \tag{1}$$

Here, $\frac{u'_j}{\Delta x}$ is an approximate slope that satisfies the second order of accuracy condition

$$\frac{u'_j}{\Delta x} = \frac{\partial}{\partial x}u(x_j, t^n) + \mathcal{O}(\Delta x). \tag{2}$$

The approximate slopes $\{u'_j\}$ are reconstructed from the known cell averages $\{\bar{u}^n_j\}$, so that they maintain second-order accuracy (2), while at the same time, they maintain a non-oscillatory property of the piece-wise linear reconstruction $u^{\Delta x}(x, t^n)$. A canonical example for such reconstructed slopes is given by the so-called minmod limiter

$$u'_j = \operatorname{minmod}\left(\Delta\bar{u}^n_{j-\frac{1}{2}}, \Delta\bar{u}^n_{j+\frac{1}{2}}\right), \qquad \Delta u^n_{j+\frac{1}{2}} := u^n_{j+1} - u^n_j, \tag{3a}$$

where $\operatorname{minmod}(\cdot,\cdot)$ is given by

$$\operatorname{minmod}(a, b) := \frac{\operatorname{sgn}(a) + \operatorname{sgn}(b)}{2} \cdot \min\{|a|, |b|\}. \tag{3b}$$

It follows that the corresponding reconstruction $u^{\Delta x}(x, t^n)$ satisfies the second-order accuracy at all by but the critical cells where $\frac{\partial}{\partial x}u(x_j, t^n) = 0$, while satisfying the TVD stability property

$$||u^{\Delta x}(\cdot, t^n)||_{\mathrm{TV}} \leqslant ||u^n||_{\mathrm{TV}} := \sum_j \left| \Delta u^n_{j+\frac{1}{2}} \right|. \tag{4}$$

We now put this second-order, TVD minmod-based reconstruction into action, in the context of approximate solution for one-dimensional nonlinear systems of conservation laws

$$\frac{\partial}{\partial t}\mathbf{u}(x,t) + \frac{\partial}{\partial x}\mathbf{f}(\mathbf{u}(x,t)) = 0, \qquad \mathbf{u}(x,t)\colon \Omega \times \mathbb{R}_+ \mapsto \mathbb{R}^k, \quad \Omega \subseteq \mathbb{R}, \tag{5}$$

where $\mathbf{f}$ is the $k$-vector of smooth flux functions. To this end, the reconstructed solution $\mathbf{u}^{\Delta x}(\cdot, t^n)$ is evolved to time $t^{n+1} = t^n + \Delta t$ by solving (5) subject to the piece-wise linear data $\mathbf{u}(\cdot, t^n) = \mathbf{u}^{\Delta x}(\cdot, t^n)$ and the resulting solution, $\mathbf{u}(x, t^{n+1})$ is then realized by its cell averages $\mathbf{u}^{n+1} = \sum_\alpha \bar{\mathbf{u}}^{n+1}_\alpha \mathbb{1}_{[x_{\alpha+\frac{1}{2}}, x_{\alpha-\frac{1}{2}}]}$. This completed the cycle of Godunov-type scheme: it consists of the reconstruction step

$$\mathcal{R}\colon \bar{\mathbf{u}}^n_\alpha = \sum_\alpha \bar{\mathbf{u}}^n_\alpha \mathbb{1}_{\left[x_{\alpha-\frac{1}{2}}, x_{\alpha+\frac{1}{2}}\right]} \mapsto \mathbf{u}^{\Delta x}(\cdot, t^n); \tag{6}_{\mathcal{R}}$$

for simplicity, we assume that the reconstruction step is carried out by implementing the piece-wise linear reconstruction (1), (2) component-wise[1]. This then is followed by the evolution step:

$$\mathcal{E}(t^n, \Delta t)\colon \mathbf{u}^{\Delta x}(\cdot, t^n) \mapsto \mathbf{u}^{n+1}(\cdot, t^{n+1}), \tag{6}_{\mathcal{E}}$$

and ending with averaging

$$\mathcal{A}\colon \mathbf{u}^{n+1}(\cdot, t^{n+1}) \mapsto \mathbf{u}^{n+1} = \sum_\alpha \bar{\mathbf{u}}^{n+1}_\alpha \mathbb{1}_{\left[x_{\alpha-\frac{1}{2}}, x_{\alpha+\frac{1}{2}}\right]}. \tag{6}_{\mathcal{A}}$$

It is well known that shock discontinuities—and in most cases of generic data—will be formed at the finite time with entropic solutions of (5). Thus, one must accept that the underlying solution is discontinuous, and a high-resolution numerical scheme should be designed, so that it prevents the spurious (Gibbs) oscillations associated with such discontinuities, particularly when high-order (order $> 1$) accuracy is involved. Since the averaging operator is inherently stable, it is the primary role of a non-oscillatory reconstruction step $\mathcal{R}$ to keep the stability compatible with the evolution step, e.g., [53]. Back to the scalar case $k = 1$, the stability is interpreted in the sense of satisfying the TVD property; then, if the reconstruction is TVD, (4) would imply the TVD stability of the overall scheme

$$\begin{aligned}
\left\| \sum_\alpha \bar{u}^{n+1}_\alpha \mathbb{1}_{\left[x_{\alpha+\frac{1}{2}}, x_{\alpha-\frac{1}{2}}\right]} \right\|_{\mathrm{TV}} &\leqslant \|\mathcal{E}(t^n, \Delta t) u^{\Delta x}(\cdot, t^n)\|_{\mathrm{TV}} \\
&\leqslant \|u^{\Delta x}(\cdot, t^n)\|_{\mathrm{TV}} \\
&\leqslant \left\| \sum_\alpha \bar{u}^n_j \mathbb{1}_{\left[x_{\alpha-\frac{1}{2}}, x_{\alpha+\frac{1}{2}}\right]} \right\|_{\mathrm{TV}} \leqslant \cdots \leqslant \left\| \sum_\alpha \bar{u}^0_\alpha \mathbb{1}_{\left[x_{\alpha-\frac{1}{2}}, x_{\alpha+\frac{1}{2}}\right]} \right\|_{\mathrm{TV}}.
\end{aligned}$$

[1] In general, one makes use of local characteristic decomposition.

**Remark 1** (Staggered grids) The last argument occupied an arbitrary index $\alpha$ to emphasize that it may vary over the integers $\alpha \leftrightarrow j \in \mathbb{Z}$ or over the half integers $\alpha = j + 1/2$, or we can even allow staggered grids with time-dependent shifts $\alpha \mapsto \alpha^n = j + (\frac{1}{2})^{n-2[n/2]}$, $j \in \mathbb{Z}$.

The TV stability encoded in the successive inequalities above highlights the pivotal role of the minmod limiter in securing the TVD stability of the overall scheme. This line of argument extends to a general class of non-oscillatory limiters which take the form

$$u'_j = \psi\left(\Delta\bar{u}^n_{j-\frac{1}{2}}, \Delta\bar{u}^n_{j+\frac{1}{2}}\right).$$

The corresponding Godunov-type scheme $u^{n+1}(x) = \mathcal{A}\mathcal{E}\mathcal{R}u^n(x)$ based on such $\psi$-limiter amounts to a 5-cell stencil[2]. The essential feature of these limiters-based reconstructions is forming difference stencils in the direction of smoothness, rather than in the direction of flow. Put differently, limiters include adaptive edge detectors which are necessary to secure a non-oscillatory reconstruction, by avoiding "crossing" of the discontinuous data. Higher order accuracy requires numerical derivatives with limiters which occupy even wider stencils, e.g., [5]

$$\psi\left(\cdots, \Delta\bar{u}^n_{j-\frac{3}{2}}, \Delta\bar{u}^n_{j-\frac{1}{2}}, \Delta\bar{u}^n_{j+\frac{1}{2}}, \Delta\bar{u}^n_{j+\frac{3}{2}}, \cdots\right),$$

which eventually led to the class of adaptive-based stencils in (W)ENO schemes [15, 18, 45]. Back to second-order resolution, the TVD criteria have a profound influence on the development of high-resolution numerical schemes, starting with the second-order flux-limiter MUSCL schemes [26, 27] and following the systematic framework for TVD stability offered in [14]. A variety of limiters have been proposed in the 1970s and have been studied in the context of TVD limiters since the 1980s. We mention two examples from the systematic study of second-order limiters found in [49]. First is the class of minmod $_\theta$ limiters

$$u'_j = \text{minmod}_\theta\left(\Delta\bar{u}^n_{j-\frac{1}{2}}, \Delta\bar{u}^n_{j+\frac{1}{2}}\right), \qquad \Delta u^n_{j+\frac{1}{2}} := u^n_{j+1} - u^n_j,$$

where minmod $_\theta$ is given by a one-parameter family of limiters

$$\text{minmod}_\theta(a,b) := \begin{cases} s \cdot \min\left(\theta|a|, \dfrac{|a+b|}{2}, \theta|b|\right), & \text{if } \text{sgn}(a) = \text{sgn}(b) := s, \\ 0, & \text{if } \text{sgn}(a) + \text{sgn}(b) = 0, \end{cases} \qquad 1 \leqslant \theta \leqslant 2. \tag{7}$$

The case $\theta = 1$ recovers the vanilla version of minmod (3b). As a second example, we mention the van Albada (vA) limiter

$$\psi^\epsilon_{\text{vA}}(a,b) = \frac{(a^2+\epsilon^2)b + (b^2+\epsilon^2)a}{a^2+b^2+2\epsilon^2}, \quad \epsilon^2 = \mathcal{O}(\Delta x^3). \tag{8}$$

[2] To be precise, the resulting scheme is "essentially 3-point" stencil in the sense that the corresponding minmod-based numerical flux $F_{j+\frac{1}{2}} = F(u_{j-1}, u_j, u_{j+1}, u_{j+2})$ satisfies $F(\cdot, \bar{u}, \bar{u}, \cdot) = f(\bar{u})$ [39].

This limiter was first proposed by van Albada et al. [1] in 1982 and has been successfully applied in computations (see, e.g., [35, 42, 47]), although a rigorous study of its TVD stability was overshadowed by widespread applications of minmod limiter. A main aspect of this paper is to prove the TVD properties of the vA limiter $\psi_{\text{vA}}$. In fact, we demonstrate that when applied to the class of high-resolution central schemes, the vA limiter yields comparable and in certain cases superior performance over the minmod limiter. This is attributed to the smoothness of the vA limiter at critical cells of local extrema[3], in contrast to the minmod limiters, where $\text{minmod}_\theta(\Delta\bar{u}_{j-\frac{1}{2}}, \Delta\bar{u}_{j+\frac{1}{2}}) = 0$ whenever $\Delta\bar{u}_{j-\frac{1}{2}} \cdot \Delta\bar{u}_{j+\frac{1}{2}} < 0$. Thus, the minmod-based polynomial reconstruction degenerates to first-order piece-wise constant interpolation at extrema cells, whereas the vA limiter still extracts more accurate information in the direction of smoothness; see (23) and (24).

## 2 Brief Review of Second-Order Central Schemes

We distinguish between two classes of Godunov-type schemes, depending on the averaging step in $(6)_{\mathcal{A}}$. In one approach, averaging at $t = t^{n+1}$ is taken at the same grid as in $t = t^n$ with $\alpha \leftrightarrow j$, $j \in \mathbb{Z}$. This leads to the class of upwind schemes which employ upstream-biased information to approximate spatial derivative. The class of the upwind scheme requires the solution of a sequence of non-interacting Riemann solvers to realize the evolution step $(6)_{\mathcal{E}}$. Wherever a second-order limiter is "turned off", the upwind scheme is reduced to the first-order Godunov scheme [11] which evolves the piece-wise constant approximate solution, based on cell averages $\{\bar{\mathbf{u}}_j^n\}$,

$$\begin{aligned}\bar{\mathbf{u}}_j^{n+1} &= \bar{\mathbf{u}}_j^n - \frac{1}{\Delta x}\int_{t^n}^{t^{n+1}} \left[\mathbf{f}\Big(\mathbf{u}^{\Delta x}(x_{j+\frac{1}{2}}, t)\Big) - \mathbf{f}\Big(\mathbf{u}^{\Delta x}(x_{j-\frac{1}{2}}, t)\Big)\right] \mathrm{d}t \\ &= \bar{\mathbf{u}}_j^n - \lambda\left(\mathbf{f}\left(\mathbf{u}^*_{j+\frac{1}{2}}\right) - \mathbf{f}\left(\mathbf{u}^*_{j-\frac{1}{2}}\right)\right),\end{aligned} \tag{9}$$

where $\lambda := \dfrac{\Delta t}{\Delta x}$ is the fixed mesh ratio. The states $\mathbf{u}^*_{j\pm\frac{1}{2}}$ are obtained with exact or approximate Riemann solvers; see, e.g., [6, 7, 16, 41, 56]. When applied to systems of equations, both left- and right-running waves may exist at interfaces. Hence, the local characteristic decomposition of the flux $\mathbf{f}$ is required for the upwind constructions, based on the "direction of the wind" identified by characteristic decomposition into local eigen-fields.

The class of central schemes keeps the averaging over the staggered grid, $\alpha \leftrightarrow j + 1/2$, $j \in \mathbb{Z}$, so that it processes the information from upstream and downstream in an averaged, "central" manner, [36, 55]. The evolution step in the class of central schemes requires simple quadrature; no Riemann solvers are needed. However, wherever a second-order limiter is "turned off"; it is reduced to the diffusive Lax-Friedrichs (LxF) scheme [25]:

$$\bar{\mathbf{u}}_{j+\frac{1}{2}}^{n+1} = \frac{\bar{\mathbf{u}}_j^n + \bar{\mathbf{u}}_{j+1}^n}{2} - \lambda\left(\mathbf{f}\left(\mathbf{u}_{j+1}^n\right) - \mathbf{f}\left(\mathbf{u}_j^n\right)\right). \tag{10}$$

[3] Specifically, the Lipschitz smoothness of $\psi_{\text{vA}}(1, r)$ as a function of $r = \frac{\Delta\bar{u}_{j-\frac{1}{2}}}{\Delta\bar{u}_{j+\frac{1}{2}}}$.

In contrast to the Godunov scheme (9), the LxF solver computes the cell averages on the staggered mesh, $\bar{\mathbf{u}}(x_{j+\frac{1}{2}},t) := \frac{1}{\Delta x}\int_{x_j}^{x_{j+1}} \mathbf{u}(x,t)\mathrm{d}x$, recalling Remark 1. The integration of (5) over the staggered control volume $[x_j,x_{j+1}]\times[t^n,t^{n+1}]$ yields

$$\bar{\mathbf{u}}\left(x_{j+\frac{1}{2}},t^{n+1}\right) = \frac{1}{\Delta x}\int_{x_j}^{x_{j+1}} \mathbf{u}(x,t^n)\mathrm{d}x - \frac{1}{\Delta x}\int_{t^n}^{t^{n+1}} [\mathbf{f}(\mathbf{u}(x_{j+1},t)) - \mathbf{f}(\mathbf{u}(x_j,t))]\mathrm{d}t. \tag{11}$$

It is clear that the LxF scheme is a first-order approximation to (11). Compared with the upwind framework, the advantage of central differencing is that the solution is smooth in the neighborhood of points $\{x_j\}$. Indeed, under a sufficiently small time step $\Delta t$, the Riemann waves initiating from $x_{j+\frac{1}{2}}$ do not affect the adjacent cell centers within the time slab, $t\in[t^n,t^{n+1}]$. Hence, the costly characteristic decompositions can be avoided.

In spite of its simplicity, the main disadvantage of the LxF scheme is the excessive numerical dissipation which reduces its resolution at discontinuities and smooth extrema. The situation is dramatically improved by applying higher order piece-wise polynomial interpolations, leading to the second-order Nessyahu-Tadmor (NT) scheme[4]. Still, wherever a minmod limiter is "turned off", the second-order central scheme is reduced to the diffusive LxF scheme. This is precisely why the gain of a smooth vA limiter over the minmod limiter is more noticeable in the context of central schemes. We turn to briefly review the second-order fully discrete and semi-discrete central schemes.

### 2.1 The Nessyahu-Tadmor (NT) Scheme

The second-order fully discrete central scheme was first proposed in 1990 [36]. The second order of accuracy is obtained by combining the $\mathcal{RECA}$ steps. First, we evolve a reconstructed piece-wise linear solution $u(x,t^n)$ (1): integration of (5) over the rectangle $[x_j,x_{j+1}]\times[t^n,t^{n+1}]$ yields

$$\begin{aligned}\bar{\mathbf{u}}_{j+\frac{1}{2}}^{n+1} =& \frac{1}{\Delta x}\left[\int_{x_j}^{x_{j+\frac{1}{2}}} \mathbf{p}_j^n(x)\mathrm{d}x + \int_{x_{j+\frac{1}{2}}}^{x_{j+1}} \mathbf{p}_{j+1}^n(x)\mathrm{d}x\right]\\ &- \frac{1}{\Delta x}\int_{t^n}^{t^{n+1}} \left[\mathbf{f}\left(\mathbf{u}^{\Delta x}(x_{j+1},t)\right) - \mathbf{f}\left(\mathbf{u}^{\Delta x}(x_j,t)\right)\right]\mathrm{d}t.\end{aligned}$$

Then, the time integral of the flux function can be approximated by the midpoint rule at the expense of $\mathcal{O}(\Delta t^3)$ local truncation error. This results in the NT scheme

$$\bar{\mathbf{u}}_{j+\frac{1}{2}}^{n+1} = \frac{\bar{\mathbf{u}}_j^n + \bar{\mathbf{u}}_{j+1}^n}{2} + \frac{1}{8}(\mathbf{u}_j' - \mathbf{u}_{j+1}') - \lambda\left[\mathbf{f}\left(\mathbf{u}_{j+1}^{n+\frac{1}{2}}\right) - \mathbf{f}\left(\mathbf{u}_j^{n+\frac{1}{2}}\right)\right]. \tag{12}$$

The midpoint values $\mathbf{u}_j^{n+\frac{1}{2}}$ are predicted by Taylor expansions

$$\mathbf{u}_j^{n+\frac{1}{2}} = \bar{\mathbf{u}}_j^n - \frac{\lambda}{2}\mathbf{f}_j',$$

[4] At the end, all fully discrete second-order accurate schemes are one version of another of the Lax-Wendroff scheme.

where the numerical derivative $f_j'$ satisfies the second-order accuracy condition

$$\frac{\mathbf{f}_j'}{\Delta x} = \frac{\partial}{\partial x}\mathbf{f}(\bar{\mathbf{u}}_j^n) + \mathcal{O}(\Delta x). \tag{13}$$

Different options of evaluating $\mathbf{f}_j'$ were proposed in [36]. For example, the numerical derivative can be computed in terms of the exact flux Jacobian

$$\mathbf{f}_j' = A(\bar{\mathbf{u}}_j^n)\mathbf{u}_j', \qquad A(\mathbf{u}) := \frac{\partial \mathbf{f}(\mathbf{u})}{\partial \mathbf{u}}. \tag{14}$$

Alternatively, one can apply Jacobian-free approximations when the characteristic decomposition is computationally expensive (even sometimes inaccessible), for example,

$$\mathbf{f}_j' = \text{minmod}\left(\Delta \mathbf{f}_{j-\frac{1}{2}}, \Delta \mathbf{f}_{j+\frac{1}{2}}\right), \qquad \Delta \mathbf{f}_{j+\frac{1}{2}} := \mathbf{f}\left(\bar{\mathbf{u}}_{j+1}^n\right) - \mathbf{f}(\bar{\mathbf{u}}_j^n). \tag{15}$$

Numerical results in [19, 33] have shown that the Jacobian-free version of the central scheme does not deteriorate the high resolution. When applied to systems of equations, the NT scheme inherits the simplicity of the LxF solver, i.e., the constructions can be extended in a component-wise manner without the use of Riemann solvers or characteristic decompositions.

The multidimensional formulation of the NT scheme was obtained with similar integration procedures, and details can be found in [2, 4, 19]. The order of accuracy can be further improved by applying higher order piece-wise polynomial interpolants; see, e.g., [28–30, 33]. Related references can be found in [3].

### 2.2 The Semi-discrete Formulation

It can be shown that the numerical dissipation of the NT scheme has order $\mathcal{O}((\Delta x)^4/\Delta t)$. In the convective problems where $\Delta t \sim \Delta x$, the NT scheme achieves higher resolution than the first-order LxF scheme due to the reduced numerical viscosity. However, it is noticed that the NT scheme and its higher order extensions do not admit any semi-discrete limits, and hence, they are not appropriate for small time step computations or steady-state calculations. This motivated the development of semi-discrete central schemes. We sketch the derivations along the lines of [23, 24].

We start with a piece-wise polynomial approximation $\mathbf{u}^{\Delta x}(x, t^n) \approx u(x, t^n)$ of the form

$$\mathbf{u}^{\Delta x}(x, t^n) = \sum_j \mathbf{p}_j^n(x)\mathbb{1}_{[x_{j-\frac{1}{2}}, x_{j+\frac{1}{2}}]}.$$

The polynomials $p_j^n(x)$ should have desired order of accuracy and conserve the cell averages $\bar{\mathbf{u}}_j^n := \bar{u}(x_j, t^n)$, that is

$$\frac{1}{\Delta x}\int_{x_{j-\frac{1}{2}}}^{x_{j+\frac{1}{2}}} \mathbf{p}_j^n(x)\mathrm{d}x = \bar{\mathbf{u}}_j^n.$$

We denote the reconstructed variables at $x_{j+\frac{1}{2}}$ from the left and the right by

$$\mathbf{u}_{j+\frac{1}{2}}^- := \mathbf{p}_j^n\left(x_{j+\frac{1}{2}}\right), \qquad \mathbf{u}_{j+\frac{1}{2}}^+ := \mathbf{p}_{j+1}^n\left(x_{j+\frac{1}{2}}\right). \tag{16}$$

In particular, when the MUSCL interpolant (1) is applied, we have

$$\mathbf{u}^{-}_{j+\frac{1}{2}} := \bar{\mathbf{u}}^{n}_{j} + \frac{1}{2}\mathbf{u}'_{j}, \quad \mathbf{u}^{+}_{j+\frac{1}{2}} := \bar{\mathbf{u}}^{n}_{j+1} - \frac{1}{2}\mathbf{u}'_{j+1}. \tag{17}$$

To obtain a semi-discrete formulation, the key idea is to take cell averaging over narrower control volumes. Assume that the maximal forward and backward wave speeds at $x_{j+\frac{1}{2}}$ are estimated by $a^{+}_{j+\frac{1}{2}} \geqslant 0$ and $a^{-}_{j+\frac{1}{2}} \leqslant 0$. At the next time level $t^{n+1} := t^{n} + \Delta t$, the region influenced by the Riemann fan originating at $x_{j+\frac{1}{2}}$ is approximated with the interval $I_{j+\frac{1}{2}} := \left[x^{-}_{j+\frac{1}{2}}, x^{+}_{j+\frac{1}{2}}\right]$, where

$$x^{+}_{j+\frac{1}{2}} := x_{j+\frac{1}{2}} + a^{+}_{j+\frac{1}{2}}\Delta t, \quad x^{-}_{j+\frac{1}{2}} := x_{j+\frac{1}{2}} + a^{-}_{j+\frac{1}{2}}\Delta t.$$

It is clear that under a sufficiently small time step, the non-smooth regions $I_{j+\frac{1}{2}}$ are separated due to the finite wave speeds. In this way, the width of Riemann fan is bounded by $\left(a^{+}_{j+\frac{1}{2}} - a^{-}_{j+\frac{1}{2}}\right)\Delta t$, in contrast to the fixed width $\Delta x$ in the fully discrete counterpart.

Now, we reconstruct a non-oscillatory, conservative, piece-wise polynomial interpolant at $t = t^{n+1}$,

$$\widetilde{\mathbf{w}}^{n+1}(x) = \sum_{j}\left[\widetilde{\mathbf{w}}^{n}_{j}(x)\mathbb{1}_{\left[x^{+}_{j-\frac{1}{2}}, x^{-}_{j+\frac{1}{2}}\right]} + \widetilde{\mathbf{w}}^{n}_{j+\frac{1}{2}}(x)\mathbb{1}_{\left[x^{-}_{j+\frac{1}{2}}, x^{+}_{j+\frac{1}{2}}\right]}\right]. \tag{18}$$

The polynomials $\widetilde{\mathbf{w}}^{n+1}_{j}$ and $\widetilde{\mathbf{w}}^{n+1}_{j+\frac{1}{2}}$ conserve the cell averages, $\bar{\mathbf{w}}^{n+1}_{j}$ and $\bar{\mathbf{w}}^{n+1}_{j+\frac{1}{2}}$, over the smooth and non-smooth domains. The values of $\bar{\mathbf{w}}^{n+1}_{j}$ and $\bar{\mathbf{w}}^{n+1}_{j+\frac{1}{2}}$ are computed by integrating (5) over the rectangular domains, $\left[x^{+}_{j-\frac{1}{2}}, x^{-}_{j+\frac{1}{2}}\right] \times [t^{n}, t^{n+1}]$ and $\left[x^{-}_{j+\frac{1}{2}}, x^{+}_{j+\frac{1}{2}}\right] \times [t^{n}, t^{n+1}]$, respectively.

Finally, the cell average at $t^{n+1}$ is computed with

$$\bar{\mathbf{u}}^{n+1}_{j} = \frac{1}{\Delta x}\int_{x_{j-\frac{1}{2}}}^{x_{j+\frac{1}{2}}} \widetilde{\mathbf{w}}^{n+1}(x)\mathrm{d}x.$$

Passing the limit $\Delta t \to 0$ yields a semi-discrete conservative scheme

$$\frac{\mathrm{d}}{\mathrm{d}t}\bar{\mathbf{u}}_{j}(t) := \lim_{\Delta t \to 0}\frac{\bar{\mathbf{u}}^{n+1}_{j} - \bar{\mathbf{u}}^{n}_{j}}{\Delta t} = -\frac{\mathbf{F}_{j+\frac{1}{2}}(t) - \mathbf{F}_{j-\frac{1}{2}}(t)}{\Delta x}, \tag{19a}$$

where the numerical fluxes $\mathbf{F}_{j+\frac{1}{2}}(t)$ are given by

$$\mathbf{F}_{j+\frac{1}{2}}(t) := \frac{a^{+}_{j+\frac{1}{2}}\mathbf{f}\left(\mathbf{u}^{-}_{j+\frac{1}{2}}\right) - a^{-}_{j+\frac{1}{2}}\mathbf{f}\left(\mathbf{u}^{+}_{j+\frac{1}{2}}\right)}{a^{+}_{j+\frac{1}{2}} - a^{-}_{j+\frac{1}{2}}} + \frac{a^{+}_{j+\frac{1}{2}}a^{-}_{j+\frac{1}{2}}}{a^{+}_{j+\frac{1}{2}} - a^{-}_{j+\frac{1}{2}}}\left(\mathbf{u}^{+}_{j+\frac{1}{2}} - \mathbf{u}^{-}_{j+\frac{1}{2}}\right). \tag{19b}$$

There are different options to estimate the wave speeds $a^{\pm}_{j+\frac{1}{2}}$. The Kurganov-Tadmor (KT) scheme proposed in [24] uses the spectral radius of the Jacobian $A(\mathbf{u}) := \dfrac{\partial \mathbf{f}(\mathbf{u})}{\partial \mathbf{u}}$,

$$a^+_{j+\frac{1}{2}} = -a^-_{j+\frac{1}{2}} = a_{j+\frac{1}{2}} := \max\left\{\rho\left(A\left(\mathbf{u}^-_{j+\frac{1}{2}}\right)\right), \rho\left(A\left(\mathbf{u}^+_{j+\frac{1}{2}}\right)\right)\right\},$$

where $\rho(\cdot)$ represents the spectral radius of a matrix. Then, the numerical flux can be expressed in terms of the Rusanov flux

$$\begin{aligned}\mathbf{F}_{j+\frac{1}{2}}(t) = \mathbf{F}^{\text{Rus}}\left(\mathbf{u}^-_{j+\frac{1}{2}}, \mathbf{u}^+_{j+\frac{1}{2}}\right) :=& \frac{\mathbf{f}\left(\mathbf{u}^-_{j+\frac{1}{2}}\right) + \mathbf{f}\left(\mathbf{u}^+_{j+\frac{1}{2}}\right)}{2} \\ &- \frac{a_{j+\frac{1}{2}}}{2}\left(\mathbf{u}^+_{j+\frac{1}{2}} - \mathbf{u}^-_{j+\frac{1}{2}}\right).\end{aligned} \tag{20}$$

For strictly hyperbolic problems, the flux Jacobian $\dfrac{\partial \mathbf{f}}{\partial \mathbf{u}}$ has $N$ distinct eigenvalues $\lambda_1 < \cdots < \lambda_N$. The semi-discrete central-upwind scheme version of KNP [23] employs a more accurate estimate of the wave speeds

$$\begin{cases} a^+_{j+\frac{1}{2}} = \max\left\{\lambda_N\left(A\left(\mathbf{u}^-_{j+\frac{1}{2}}\right)\right), \lambda_N\left(A\left(\mathbf{u}^+_{j+\frac{1}{2}}\right)\right), 0\right\}, \\ a^-_{j+\frac{1}{2}} = \min\left\{\lambda_1\left(A\left(\mathbf{u}^-_{j+\frac{1}{2}}\right)\right), \lambda_1\left(A\left(\mathbf{u}^+_{j+\frac{1}{2}}\right)\right), 0\right\}. \end{cases} \tag{21}$$

In this way, the scheme reduces the numerical dissipation by employing the HLL flux [17].

In the computations, the set of ODEs (19) is integrated with an appropriate ODE solver. To preserve the overall high order of accuracy as well as the non-oscillatory property, one may apply a higher order Strong Stability Preserving (SSP) Runge-Kutta method; see, e.g., [12, 13, 44, 48].

The semi-discrete central schemes retain the advantage of being Riemann-solver-free, and hence, the component-wise extension is allowed when solving systems of equations. In multidimensional problems, the second-order constructions can be extended in a dimension-by-dimension manner. Third-order extensions have also been derived with the help of piece-wise parabolic interpolants; we refer to the details in [22, 24].

## 3 Analysis of the Smooth vA Limiter

In this section, we study the analytical properties of the smooth vA limiter (8). To get more insight, the limiter can be written as [26]

$$\psi^{\epsilon}_{\text{vA}}(a,b) = \frac{a+b}{2}\left(1 - \frac{(a-b)^2}{a^2+b^2+2\epsilon^2}\right).$$

In the smooth regions where $a \approx b$, the limiter tends to recover the second-order central finite differencing $\dfrac{a+b}{2}$. Across the discontinuities, however, the averaged slope is biased to the smallest value among the two one-sided slopes. These mechanisms are expected to ensure the second-order accuracy and prevent the undesirable numerical oscillations. We will provide rigorous proofs for these advantages. For convenience of discussion, we will consider the simplified version without $\epsilon$,

$$\psi_{\mathrm{vA}}(a,b) = \frac{a^2 b + ab^2}{a^2 + b^2}, \quad a^2 + b^2 \neq 0. \tag{22}$$

Indeed, as reported in [1], the computed solutions are not sensitive to the specific value of $\epsilon$.

### 3.1 The Second-Order Accuracy

We show that the vA limiter (22) ensures a second-order spatial accuracy. Back in the scalar framework, we first consider the reconstruction based on the point values $u_j := u(x_j)$. Denote the left- and the right-sided slopes by

$$\partial_x^- u_j := \frac{u_j - u_{j-1}}{\Delta x} \quad \text{and} \quad \partial_x^+ u_j := \frac{u_{j+1} - u_j}{\Delta x}.$$

The numerical derivative constructed with the vA limiter (22) is given by

$$\frac{u_j'}{\Delta x} = \frac{(\partial_x^- u_j)(\partial_x^+ u_j)^2 + (\partial_x^+ u_j)(\partial_x^- u_j)^2}{(\partial_x^+ u_j)^2 + (\partial_x^- u_j)^2}.$$

The Taylor expansion yields

$$\frac{u_j'}{\Delta x} = \partial_x u_j + \left(\frac{1}{6}\partial_x^3 u_j - \frac{1}{2}\frac{(\partial_x^2 u_j)^2}{\partial_x u_j}\right)\Delta x^2 + \mathcal{O}(\Delta x^3). \tag{23}$$

The second-order condition (2) is satisfied in regions away from critical points $|\partial_x u_j| \gg \Delta x$. In the framework of finite-volume methods, the slope reconstruction is based on the cell averages $\bar{u}_j := \frac{1}{\Delta x}\int_{x_{j-\frac{1}{2}}}^{x_{j+\frac{1}{2}}} u(x)\mathrm{d}x$. Then, the Taylor expansion is slightly modified

$$\frac{u_j'}{\Delta x} = \partial_x u_j + \left(\frac{1}{6}\partial_x^3 u_j + \frac{1}{24}\partial_x^4 u_j - \frac{1}{2}\frac{\partial_x^2 u_j}{\partial_x u_j}\right)\Delta x^2 + \mathcal{O}(\Delta x^3), \qquad |\partial_x u_j| \gg \Delta x. \tag{24}$$

For both point-value-based and cell-average-based reconstructions, the numerical derivative $u_j'/\Delta x$, approximates the exact derivative $\partial_x u_j$ with order $\mathcal{O}(\Delta x^2)$ in the non-critical regions. Near the critical points, the second-order condition (2) is satisfied up to $\partial_x u \approx \Delta x$. Hence, it is expected that the vA limiter introduces less dissipation than the minmod limiter at discontinuities and smooth extrema. Their numerical performances will be compared in Sect. 4.

### 3.2 The Non-oscillatory Property

We are going to show that the vA limiter, as applied to the central schemes, generates non-oscillatory solutions. We begin with the following lemma.

**Lemma 1** *The approximate slope* $u'_j = \psi_{\mathrm{vA}}(\Delta\bar{u}_{j-\frac{1}{2}}, \Delta\bar{u}_{j+\frac{1}{2}})$ *satisfies the following estimates*:

$$\frac{1-\sqrt{2}}{2} \leqslant \frac{u'_j}{\Delta\bar{u}_{j\pm\frac{1}{2}}} \leqslant \frac{1+\sqrt{2}}{2}, \tag{25a}$$

$$\frac{|u'_{j+1} - u'_j|}{|\Delta\bar{u}_{j+\frac{1}{2}}|} \leqslant \sqrt{2}. \tag{25b}$$

**Proof** Denote $r := \dfrac{\Delta\bar{u}_{j-\frac{1}{2}}}{\Delta\bar{u}_{j+\frac{1}{2}}}$, then we can write

$$u'_j = \frac{r^2+r}{r^2+1}\Delta\bar{u}_{j+\frac{1}{2}} = \frac{r+1}{r^2+1}\Delta\bar{u}_{j-\frac{1}{2}}.$$

We will show that $\dfrac{1-\sqrt{2}}{2} \leqslant \dfrac{r^2+r}{r^2+1}, \dfrac{r+1}{r^2+1} \leqslant \dfrac{1+\sqrt{2}}{2}$.

Assume that $\dfrac{r^2+r}{r^2+1}$ is bounded from below and above by $m$ and $M \in \mathbb{R}$, respectively,

$$m \leqslant \frac{r^2+r}{r^2+1} \leqslant M, \quad \forall r \in \mathbb{R}.$$

This can be equivalently expressed as

$$\begin{cases} (M-1)r^2 - r + M \geqslant 0, \\ (m-1)r^2 - r + m \leqslant 0, \end{cases} \qquad \forall r \in \mathbb{R}. \tag{26}$$

The upper bound $M$ should satisfy the conditions

$$\begin{cases} M > 1, \\ \Delta = 1 - 4M(M-1) \leqslant 0. \end{cases}$$

Solving these inequalities yields $M \geqslant \dfrac{1+\sqrt{2}}{2}$, and hence, $\dfrac{1+\sqrt{2}}{2}$ gives the supremum of $\dfrac{r^2+r}{r^2+1}$. On the other hand, the lower bound $m$ should satisfy

$$\begin{cases} m < 1, \\ \Delta = 1 - 4m(m-1) \leqslant 0. \end{cases}$$

These conditions yield $m \leqslant \dfrac{1-\sqrt{2}}{2}$ and hence $\dfrac{1-\sqrt{2}}{2}$ gives the infimum of $\dfrac{r^2+r}{r^2+1}$. Combining these results, we have

$$\frac{1-\sqrt{2}}{2} \leqslant \frac{u'_j}{\Delta \bar{u}_{j+\frac{1}{2}}} = \frac{r^2+r}{r^2+1} \leqslant \frac{1+\sqrt{2}}{2}.$$

With similar argument, we can show that $\frac{1-\sqrt{2}}{2} \leqslant \frac{r+1}{r^2+1} \leqslant \frac{1+\sqrt{2}}{2}$, and therefore

$$\frac{1-\sqrt{2}}{2} \leqslant \frac{u'_j}{\Delta \bar{u}_{j-\frac{1}{2}}} = \frac{r+1}{r^2+1} \leqslant \frac{1+\sqrt{2}}{2}.$$

This completes the proof of (25a). The second estimate (25b) is a direct consequence of (25a).

With the help of Lemma 1, we discuss the non-oscillatory property of the fully discrete and the semi-discrete schemes separately.

### 3.2.1 The Fully Discrete Scheme

We consider the fully discrete NT scheme (12). The scheme can be written in a conservative form [36][5]

$$\bar{u}^{n+1}_{j+\frac{1}{2}} = \frac{\bar{u}^n_j + \bar{u}^n_{j+1}}{2} - \lambda(g_{j+1} - g_j), \qquad \lambda = \frac{\Delta t}{\Delta x} \tag{27}$$

with the so-called modified numerical flux $g_j$ given by

$$g_j = f\left(u_j^{n+\frac{1}{2}}\right) + \frac{1}{8\lambda} u'_j. \tag{28}$$

The NT scheme combined with the vA limiter (22) can be shown to be TVD following similar approach in [36, 39]. The proof is based on the following lemma.

**Lemma 2** ([36]) *The scheme* (12) *is TVD if the numerical flux $g_j$ satisfies the following generalized CFL condition*:

$$\lambda \left| \frac{\Delta g_{j+\frac{1}{2}}}{\Delta \bar{u}^n_{j+\frac{1}{2}}} \right| \leqslant \frac{1}{2}, \quad \Delta g_{j+\frac{1}{2}} := g_{j+1} - g_j. \tag{29}$$

**Proof** By (27), the difference $\bar{u}^{n+1}_{j+\frac{1}{2}} - \bar{u}^{n+1}_{j-\frac{1}{2}}$ amounts to

$$\bar{u}^{n+1}_{j+\frac{1}{2}} - \bar{u}^{n+1}_{j-\frac{1}{2}} = \left(\frac{1}{2} - \lambda \frac{\Delta g_{j+\frac{1}{2}}}{\Delta \bar{u}_{j+\frac{1}{2}}}\right) \Delta \bar{u}_{j+\frac{1}{2}} + \left(\frac{1}{2} + \lambda \frac{\Delta g_{j-\frac{1}{2}}}{\Delta \bar{u}_{j-\frac{1}{2}}}\right) \Delta \bar{u}_{j-\frac{1}{2}}.$$

Condition (30) implies that the coefficients in the parenthesis are positive. Hence

[5] Recall that $\lambda$ is the fixed mesh-ratio $\lambda = \frac{\Delta t}{\Delta x}$, which should be distinguished from the eigenvalues in (21), $\lambda_1 < \cdots < \lambda_N$.

$$\begin{aligned}\sum_j \left|\bar{u}^{n+1}_{j+\frac{1}{2}} - \bar{u}^{n+1}_{j-\frac{1}{2}}\right| &\leqslant \sum_j \left(\frac{1}{2} - \lambda\frac{\Delta g_{j+\frac{1}{2}}}{\Delta\bar{u}_{j+\frac{1}{2}}}\right)|\Delta\bar{u}_{j+\frac{1}{2}}| + \left(\frac{1}{2} + \lambda\frac{\Delta g_{j-\frac{1}{2}}}{\Delta\bar{u}_{j-\frac{1}{2}}}\right)|\Delta\bar{u}_{j-\frac{1}{2}}| \\ &= \sum_j \left(\frac{1}{2} - \lambda\frac{\Delta g_{j+\frac{1}{2}}}{\Delta\bar{u}_{j+\frac{1}{2}}}\right)|\Delta\bar{u}_{j+\frac{1}{2}}| + \left(\frac{1}{2} + \lambda\frac{\Delta g_{j+\frac{1}{2}}}{\Delta\bar{u}_{j-\frac{1}{2}}}\right)|\Delta\bar{u}_{j+\frac{1}{2}}| \\ &= \sum_j |\Delta\bar{u}_{j+\frac{1}{2}}|.\end{aligned}$$

We conclude $\mathrm{TV}(\bar{u}^{n+1}) \leqslant \mathrm{TV}(\bar{u}^n)$.

Equipped with Lemmas 1 and 2, we prove the NT scheme is TVD.

**Theorem 1** (TVD Stability of NT Scheme with the vA Limiter) *Consider the scalar NT scheme* (27) *using the numerical slope $u'_j$ constructed with the vA limiter* (22)*, and let the flux numerical derivative be chosen by $f'_j = a(\bar{u}^n_j)u'_j$ with $a(u) := f'(u)$. Assume that the following CFL condition is satisfied*:

$$\lambda \max_u |a(u)| \leqslant \frac{-1 + \sqrt{\frac{3}{2} + \frac{3\sqrt{2}}{4}}}{1 + \sqrt{2}} \approx 0.24. \tag{30}$$

*Then, the NT scheme* (27) *is TVD.*

**Proof** Denote $\mathrm{CFL} := \lambda \max_u |a(u)|$. By (28), we have

$$\lambda\left|\frac{\Delta g_{j+\frac{1}{2}}}{\Delta\bar{u}_{j+\frac{1}{2}}}\right| \leqslant \underbrace{\lambda\left|\frac{f\left(u^{n+\frac{1}{2}}_{j+1}\right) - f\left(u^{n+\frac{1}{2}}_{j}\right)}{u^{n+\frac{1}{2}}_{j+1} - u^{n+\frac{1}{2}}_{j}}\right|}_{\mathrm{I}} \underbrace{\left|\frac{u^{n+\frac{1}{2}}_{j+1} - u^{n+\frac{1}{2}}_{j}}{\Delta\bar{u}_{j+\frac{1}{2}}}\right|}_{\mathrm{II}} + \underbrace{\frac{1}{8}\left|\frac{\Delta u'_{j+\frac{1}{2}}}{\Delta\bar{u}_{j+\frac{1}{2}}}\right|}_{\mathrm{III}}. \tag{31}$$

By definition, the first term on the right of (31) is bounded by

$$\lambda\left|\frac{f\left(u^{n+\frac{1}{2}}_{j+1}\right) - f\left(u^{n+\frac{1}{2}}_{j}\right)}{u^{n+\frac{1}{2}}_{j+1} - u^{n+\frac{1}{2}}_{j}}\right| \leqslant \lambda \max_u |a(u)| := \mathrm{CFL}. \tag{32}$$

Notice that (25a) implies $\left|\frac{u'_j}{\Delta\bar{u}_{j\pm\frac{1}{2}}}\right| \leqslant \frac{1+\sqrt{2}}{2}$, we can estimate the second term on the right of (31),

$$\begin{aligned}\left|\frac{u^{n+\frac{1}{2}}_{j+1} - u^{n+\frac{1}{2}}_{j}}{\Delta\bar{u}_{j+\frac{1}{2}}}\right| &\leqslant 1 + \frac{\lambda}{2}\left|\frac{\Delta f'_{j+\frac{1}{2}}}{\Delta\bar{u}_{j+\frac{1}{2}}}\right| \leqslant 1 + \frac{\lambda}{2}\frac{|a_{j+1}u'_{j+1}| + |a_j u'_j|}{|\Delta\bar{u}_{j+\frac{1}{2}}|} \\ &\leqslant 1 + \frac{\lambda\max_u |a(u)|}{2}\cdot\frac{|u'_{j+1}| + |u'_j|}{|\Delta\bar{u}_{j+\frac{1}{2}}|} \leqslant 1 + \frac{1+\sqrt{2}}{2}\mathrm{CFL}.\end{aligned} \tag{33}$$

As a direct consequence of (25b), the third term on the right of (31) does not exceed

$$\frac{1}{8}\left|\frac{\Delta u'_{j+\frac{1}{2}}}{\Delta \bar{u}_{j+\frac{1}{2}}}\right| \leqslant \frac{\sqrt{2}}{8}. \tag{34}$$

Using (32), (33), and (34), the TVD condition (29) boils down to

$$\mathrm{CFL}\left(1+\frac{1+\sqrt{2}}{2}\mathrm{CFL}\right)+\frac{\sqrt{2}}{8} \leqslant \frac{1}{2},$$

which in turn recovers the CFL condition (30).

**Remark 2** The TVD stability is not sharp in the sense that the CFL condition (30) is too restrictive, and serves here only as a theoretically sufficient bound. The numerical experiments reported in Sect. 4 indicate that the computed NT solutions with the vA limiter remain non-oscillatory as long as $\mathrm{CFL} \leqslant 1/2$.

### 3.2.2 The Semi-discrete Scheme

The TVD stability of the vA limiter as applied to the non-staggered semi-discrete schemes (19) can be shown following the lines of [38, 51]. The key ingredient is to represent the scheme in an appropriate incremental form which meets a certain positive condition. We prove the following result with the help of Lemma 1.

**Theorem 2** (TVD Stability of Semi-discrete MUSCL Scheme with the vA Limiter) *Let the states* $u^{\pm}_{j+\frac{1}{2}}$ *be computed from the MUSCL reconstruction* (17) *with the numerical slope* $u'_j$ *constructed with the vA limiter* (22). *Consider a generalized scalar MUSCL scheme*

$$\frac{\mathrm{d}}{\mathrm{d}t}\bar{u}_j(t) = -\frac{1}{\Delta x}\left[F\left(u^-_{j+\frac{1}{2}}, u^+_{j+\frac{1}{2}}\right) - F\left(u^-_{j-\frac{1}{2}}, u^+_{j-\frac{1}{2}}\right)\right], \tag{35}$$

*and let the numerical flux* $F(\cdot,\cdot)$ *be monotone and consistent*

$$\frac{\partial}{\partial u}F(u,v) \geqslant 0 \quad \textit{and} \quad \frac{\partial}{\partial v}F(u,v) \leqslant 0, \tag{36a}$$

$$F(u,u) = f(u). \tag{36b}$$

*Then, the scheme* (35) *is TVD*

$$\frac{\mathrm{d}}{\mathrm{d}t}[\mathrm{TV}(\bar{u}(t))] \leqslant 0.$$

**Proof** We argue along the lines of [51], expressing the scheme (35) in the incremental form

$$\frac{\mathrm{d}}{\mathrm{d}t}\bar{u}_j = -\frac{1}{\Delta x_j}C_{j-\frac{1}{2}}\Delta \bar{u}_{j-\frac{1}{2}} + \frac{1}{\Delta x_j}D_{j+\frac{1}{2}}\Delta \bar{u}_{j+\frac{1}{2}}, \tag{37}$$

where

$$\begin{cases} C_{j-\frac{1}{2}} = \frac{1}{\Delta \bar{u}_{j-\frac{1}{2}}}\left[F\left(u^-_{j+\frac{1}{2}}, u^+_{j-\frac{1}{2}}\right) - F\left(u^-_{j-\frac{1}{2}}, u^+_{j-\frac{1}{2}}\right)\right], \\ D_{j+\frac{1}{2}} = -\frac{1}{\Delta \bar{u}_{j+\frac{1}{2}}}\left[F\left(u^-_{j+\frac{1}{2}}, u^+_{j+\frac{1}{2}}\right) - F\left(u^-_{j+\frac{1}{2}}, u^+_{j-\frac{1}{2}}\right)\right]. \end{cases} \tag{38}$$

We denote

$$s_{j+\frac{1}{2}} := \operatorname{sgn}(\Delta \bar{u}_{j+\frac{1}{2}}) = \begin{cases} 1, & \Delta \bar{u}_{j+\frac{1}{2}} > 0, \\ \pm 1, & \Delta \bar{u}_{j+\frac{1}{2}} = 0, \\ -1, & \Delta \bar{u}_{j+\frac{1}{2}} < 0, \end{cases}$$

$$\chi_j := 1 - s_{j-\frac{1}{2}} s_{j+\frac{1}{2}} = \begin{cases} 2, & \Delta \bar{u}_{j-\frac{1}{2}} \cdot \Delta \bar{u}_{j+\frac{1}{2}} \leqslant 0, \\ 0, & \Delta \bar{u}_{j-\frac{1}{2}} \cdot \Delta \bar{u}_{j+\frac{1}{2}} > 0. \end{cases}$$

Forward differencing of (37) gives

$$\begin{aligned} \frac{\mathrm{d}}{\mathrm{d}t}\Delta \bar{u}_{j+\frac{1}{2}} =& \left(\frac{1}{\Delta x_{j+1}} D_{j+\frac{3}{2}} \Delta \bar{u}_{j+\frac{3}{2}} - \frac{1}{\Delta x_{j+1}} C_{j+\frac{1}{2}} \Delta \bar{u}_{j+\frac{1}{2}}\right) \\ & - \left(\frac{1}{\Delta x_j} D_{j+\frac{1}{2}} \Delta \bar{u}_{j+\frac{1}{2}} - \frac{1}{\Delta x_j} C_{j-\frac{1}{2}} \Delta \bar{u}_{j-\frac{1}{2}}\right). \end{aligned} \tag{39}$$

Multiplying (39) by $s_{j+\frac{1}{2}}$ and summing by parts, we have

$$\begin{aligned} \frac{\mathrm{d}}{\mathrm{d}t}\mathrm{TV}(\bar{u}(t)) &= \sum_j s_{j+\frac{1}{2}} \frac{\mathrm{d}}{\mathrm{d}t}\Delta \bar{u}_{j+\frac{1}{2}} \\ &= -\sum_j \frac{1}{\Delta x}\left[\left(s_{j-\frac{1}{2}} - s_{j+\frac{1}{2}}\right) C_{j-\frac{1}{2}} \Delta \bar{u}_{j-\frac{1}{2}} + \left(s_{j+\frac{1}{2}} - s_{j-\frac{1}{2}}\right) D_{j+\frac{1}{2}} \Delta \bar{u}_{j+\frac{1}{2}}\right] \\ &= -\sum_j \frac{\chi_j}{\Delta x}\left[C_{j-\frac{1}{2}} |\Delta \bar{u}_{j-\frac{1}{2}}| + D_{j+\frac{1}{2}} |\Delta \bar{u}_{j+\frac{1}{2}}|\right]. \end{aligned}$$

Here, we use the property that $s^2_{j+\frac{1}{2}} \equiv 1$. Since $\chi_j \geqslant 0$, it suffices to show that $C_{j-\frac{1}{2}}$, $D_{j+\frac{1}{2}} \geqslant 0$. Indeed, we find that

$$\begin{cases} C_{j-\frac{1}{2}} = \partial_u F\left(\tilde{u}_1, u^+_{j-\frac{1}{2}}\right)\left(1 + \frac{u'_j - u'_{j-1}}{2\Delta \bar{u}_{j-\frac{1}{2}}}\right), \\ D_{j+\frac{1}{2}} = -\partial_v F\left(u^-_{j+\frac{1}{2}}, \tilde{u}_2\right)\left(1 - \frac{u'_{j+1} - u'_j}{2\Delta \bar{u}_{j+\frac{1}{2}}}\right), \end{cases} \tag{40}$$

where $\tilde{u}_1$ is between $u^-_{j-\frac{1}{2}}$ and $u^-_{j+\frac{1}{2}}$, and $\tilde{u}_2$ is between $u^+_{j-\frac{1}{2}}$ and $u^+_{j+\frac{1}{2}}$. From (25b), we know that the terms in the parentheses are positive. Hence, the non-negativity of $C_{j-\frac{1}{2}}$ and $D_{j+\frac{1}{2}}$ follows from (36a).

The semi-discrete central scheme (19) can be considered as a generalized MUSCL scheme, and the associated numerical flux (19b) can expressed in the form $F_{j+\frac{1}{2}}(t) := F(u^-_{j+\frac{1}{2}}, u^+_{j+\frac{1}{2}})$ with

$$F(u,v)=\frac{a^+f(u)-a^-f(v)}{a^+-a^-}+\frac{a^+a^-}{a^+-a^-}(v-u).$$

The monotonicity of $F(\cdot,\cdot)$ is clear, since $a^-\leqslant f'(u)$, $f'(v)\leqslant a^+$. Hence, the TVD stability of the vA limiter as applied to the semi-discrete central scheme (19) follows from Theorem 2.

**Remark 3** The semi-discrete scheme (19) [or equivalently (35)] advanced with forward Euler time-stepping reads

$$\bar{u}_j^{n+1}=\bar{u}_j^n-\lambda\left(F\left(u^-_{j+\frac{1}{2}},u^+_{j+\frac{1}{2}}\right)-F\left(u^-_{j-\frac{1}{2}},u^+_{j-\frac{1}{2}}\right)\right),\tag{41}$$

where $u^+_{j+\frac{1}{2}}:=\bar{u}_j^n-\frac{1}{2}u'_{j+1}$ and $u^-_{j+\frac{1}{2}}:=\bar{u}_j^n+\frac{1}{2}u'_j$. With similar incremental representation in Theorem 2, it can be proved that the vA limiter as applied to the fully discrete non-staggered scheme (41) generates TVD solutions. Applying a higher order SSP time integration method would achieve a higher order of accuracy in time without deteriorating the stability.

## 4 Numerical Experiments

In this section, we examine the performance of the vA limiter (8) with the small[6] bias, $\epsilon=(\Delta x)^3$, compared vs. the minmod limiter (7) which is taken, unless otherwise stated, in its vanilla version $\theta=1$. The advantage of the vA limiter over $\text{minmod}_1$ is apparent for both—the fully discrete NT scheme (12) and the semi-discrete central-upwind version of KNP, (19), (21).

In all the simulations of the NT scheme, the numerical slope of flux $\mathbf{f}'_j$ is evaluated with the exact flux Jacobian (14), and the CFL number is taken to be 0.45. The implementation of the semi-discrete scheme requires a high-order time discretization. We use the third-order, explicit SSPRK3 method for the time integration of method-of-lines ODEs (19a) with the CFL number chosen to be 0.7. To better ensure the robustness in the strong shock problems, the MUSCL reconstruction for systems of equations is performed on the characteristic variables, e.g., [36, (4.7)–(4.11)], [45, Procedure 2.8][7].

### 4.1 One-Dimensional Linear Advection Equation

We consider the one-dimensional linear advection equation

[6] Even smaller than the one indicated in (8); this does not seem to affect the results.

[7] Here, we use standard characteristic decomposition, $\Delta\mathbf{u}_{j+\frac{1}{2}}=\sum_k\widehat{\alpha}^k_{j+\frac{1}{2}}\widehat{\mathbf{R}}^k_{j+\frac{1}{2}}$, where $\{\widehat{\mathbf{R}}^k_{j+\frac{1}{2}}\}_k$ is the eigensystem of an intermediate Jacobian: for convenience, $\widehat{\mathbf{R}}^k_{j+\frac{1}{2}}$ are computed as the eigensystems at the arithmetic average, $A\left(\frac{1}{2}(\mathbf{u}_j+\mathbf{u}_{j+1})\right)$, rather than the Roe average, $\Delta\mathbf{f}_{j+\frac{1}{2}}=A^{\text{Roe}}_{j+\frac{1}{2}}\Delta\mathbf{u}_{j+\frac{1}{2}}$, as it does not seem to affect the MUSCL results in this context.

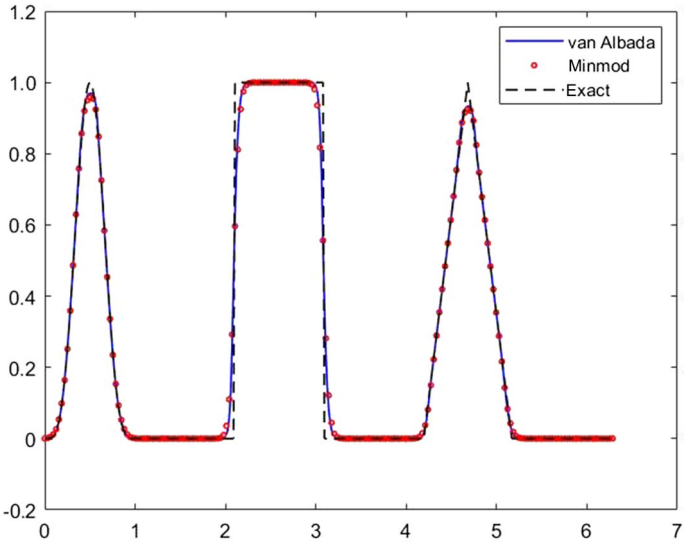


**Fig. 1** Linear advection. NT scheme, $N = 400$, periodic BCs, $t = 2\pi$

$$\frac{\partial u}{\partial t} + \frac{\partial u}{\partial x} = 0, \qquad 0 \leqslant x \leqslant 2\pi,$$

subject to the initial data

$$u(x,0)\begin{cases} = \sin^4(\pi x), & 0 \leqslant x \leqslant 1, \\ \equiv 1, & 2.09 \leqslant x \leqslant 3.09, \\ = \text{hat function with height} = 1, & 4.18 \leqslant x \leqslant 5.18, \\ \equiv 0, & \text{elsewhere in } (1, 2\pi), \end{cases}$$

and $2\pi$ periodic boundary conditions (BCs). We compute the solution after one period of revolution using $N = 400$ equi-spaced mesh grids. Figure 1 displays the solutions computed with the NT scheme. Both the vA limiter and the minmod limiter generate non-oscillatory solutions with the comparable resolution at the shocks and smooth extrema. Figure 2 compares the solutions computed with different limiters as applied to the semi-discrete central-upwind scheme. In this case, applying the smoother vA limiter improves the noticeable "clipping" of the $\text{minmod}_1$ that occurred at the peaks of the sinusoidal wave and the triangular wave.

**Remark 4** (On the superior resolution of NT with the vA limiter) It is instructive to compare the NT results in Fig. 1 which are found to be superior to the corresponding results of the central-upwind KT scheme in Fig. 2. In particular, a direct comparison in Fig. 3 shows that the "clipping" phenomenon in the three peaks is clearly stronger in the KT computation, whereas the NT scheme produces sharper peaks. We recall that the NT with minmod limiter is reduced at peaks to a diffusive LxF scheme. Thus, the vA limiter helps improve the NT resolution at peaks. Of course, the truncation error of NT schemes of order

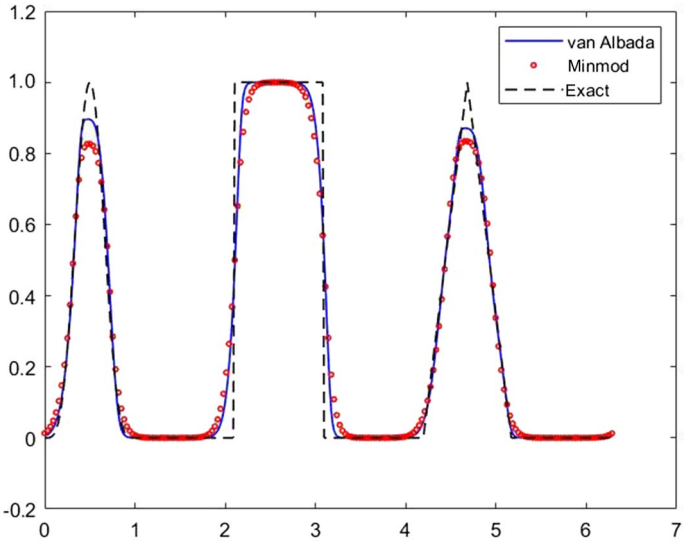


**Fig. 2** Linear advection. Semi-discrete central-upwind scheme, $N = 400$, periodic BCs, $t = 2\pi$

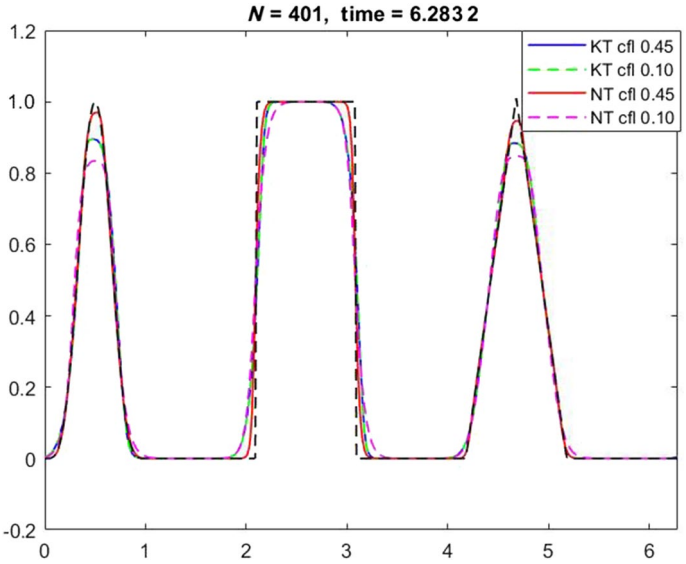


**Fig. 3** Linear advection. NT vs. semi-discrete KT scheme with vA limiter with $N = 400$ mesh points, periodic BCs at $t = 2\pi$

$\mathcal{O}((\Delta x)^2/\lambda)$ implies that the NT resolution decreases for small(er) CFL. However, for near optimal CFL = 0.45, the resolution of the NT scheme with the vA limiter offers a competitive alternative to central-upwind schemes. This conclusion will be confirmed with linear contact waves studied in Sect. 4.3.

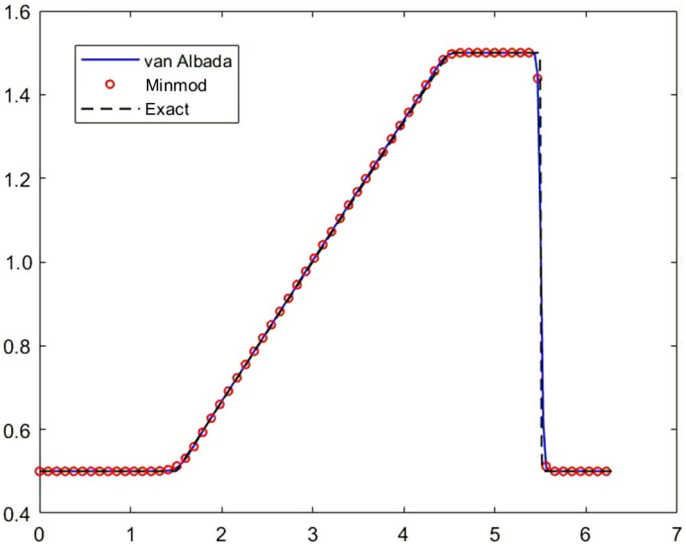


**Fig. 4** One-dimensional Burger's equation, NT scheme, $N = 200$, $t = 2$

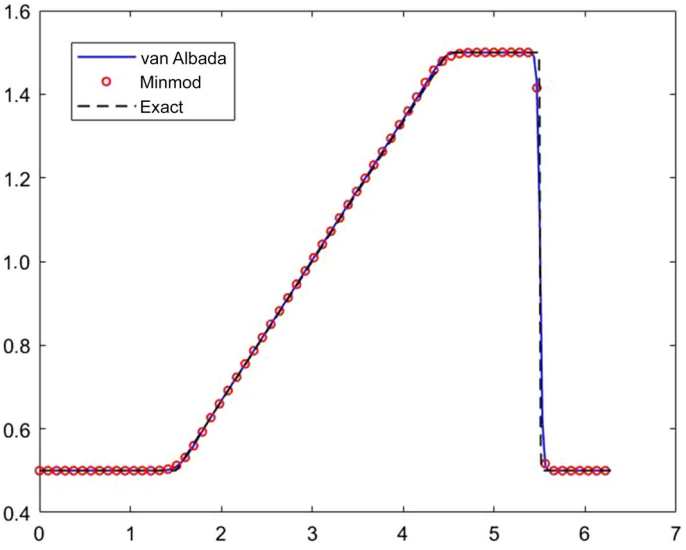


**Fig. 5** One-dimensional Burgers' equation, semi-discrete central-upwind scheme, $N = 200$, $t = 2$

### 4.2 One-Dimensional Burgers' Equation

We show the results for the one-dimensional Burgers' equation

$$\frac{\partial u}{\partial t} + \frac{\partial}{\partial x}\left(\frac{u^2}{2}\right) = 0$$

over the domain $[0, 2\pi]$. In this test case, the solution comprises of an expansion wave and a compression wave. Figures 4 and 5 present the solutions computed with $N = 200$ mesh grids at $t = 2$. In both fully discrete and semi-discrete test cases, the solutions generated with the vA limiter capture the expansion wave and the shock wave with the sharp resolution and without generating numerical oscillations. The results based on the vA limiter are essentially comparable to those based on the minmod limiter.

### 4.3 One-Dimensional Euler Equations

We consider the one-dimensional Euler equations of gas dynamics

$$\frac{\partial}{\partial t}\begin{bmatrix}\rho\\ \rho u\\ E\end{bmatrix}+\frac{\partial}{\partial x}\begin{bmatrix}\rho u\\ \rho u^2+p\\ (E+p)u\end{bmatrix}=0,$$

where $\rho$, $u$, and $p$ are the density, velocity, and pressure, respectively, and $E$ is the total energy per unit volume given by

$$E=\frac{p}{\gamma-1}+\frac{\rho u^2}{2},\quad \gamma=1.4.$$

As the first test case, we consider the Sod's shock tube problem: the computational domain is [0, 1] with an interface at $x = 0.5$, and subject to initial states on the two sides of the interface given by

$$\begin{cases} p_{\rm L}=1.0, & p_{\rm R}=0.1,\\ \rho_{\rm L}=1.0, & \rho_{\rm R}=0.125,\\ u_{\rm L}=0.0, & u_{\rm R}=0.0.\end{cases}$$

Figures 6 and 7 show the computed density at $t = 0.2$ with $N = 400$ mesh grids, computed with the NT and, respectively, semi-discrete central-upwind schemes. The numerical results comparing the vA and minmod$_1$ limiters show that the high resolution of the computation based on the vA limiter is on par with those based on the minmod limiter. In fact, we observe that the contact wave in Fig. 6 is even slightly better resolved by the NT+vA limiter compared with the central-upwind KNP+vA limiter in Fig. 7. This agrees with the improved resolution of the NT+vA limiter of linear advection discussed in Remark 4 and similar remark regarding the diffusion of the semi-discrete central-upwind KT schemes which goes back to [24, p. 268].

Next, we turn to a second test case of the Osher-Shu problem. The computational domain is $[-5, 5]$ with the interface placed at $x = -4$, subject to the initial data

$$\begin{cases} p_{\rm L}=10.333\,33, & p_{\rm R}=1.0,\\ \rho_{\rm L}=3.857\,143, & \rho_{\rm R}=1+0.2\sin(5x),\\ u_{\rm L}=2.629\,369, & u_{\rm R}=0.0.\end{cases}$$

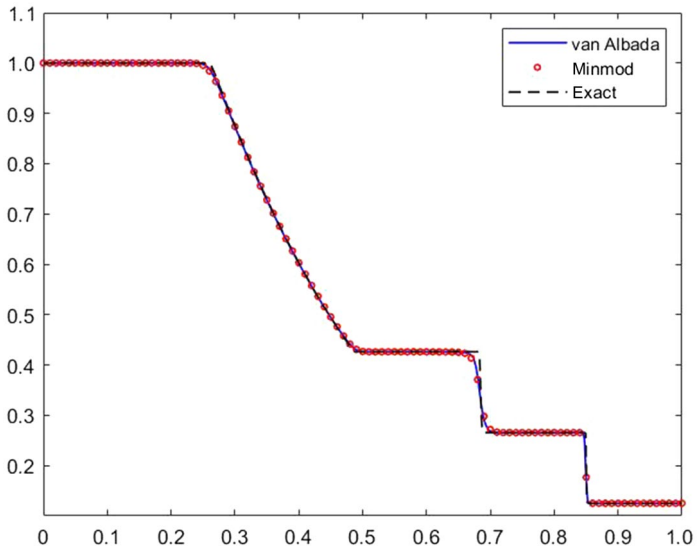


**Fig. 6** Sod's problem—density computed with NT scheme and vA limiter, $N = 400$, $t = 0.2$

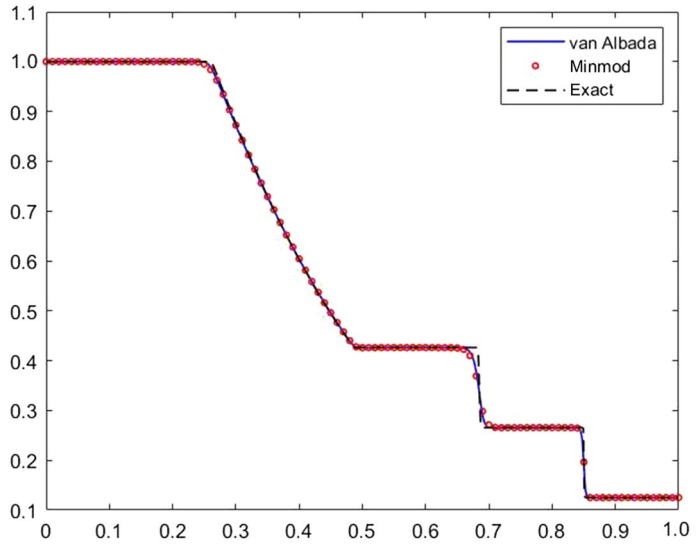


**Fig. 7** Sod's problem—density computed with semi-discrete central-upwind scheme and vA limiter, $N = 400$, $t = 0.2$

In this problem, the solution of density consists of a discontinuity and a smooth harmonic waves. Figures 6 and 9 present the solutions of density given by the NT scheme and the semi-discrete central-upwind scheme computed with $N = 600$ mesh grids at $t = 1.8$. We

observe that the solutions computed with the vA limiter resolve the smooth extremum better than those computed with the minmod limiter; in particular, the solutions do not introduce spurious numerical oscillations at the location of the shock.

### 4.4 Two-Dimensional Euler Equations

We examine the performance of the vA limiter in two-dimensional problems. We consider the double Mach reflection problem [58] for the two-dimensional Euler equations

$$\frac{\partial}{\partial t}\begin{bmatrix}\rho\\ \rho u\\ \rho v\\ E\end{bmatrix}+\frac{\partial}{\partial x}\begin{bmatrix}\rho u\\ \rho u^2+p\\ \rho uv\\ (E+p)u\end{bmatrix}+\frac{\partial}{\partial y}\begin{bmatrix}\rho v\\ \rho uv\\ \rho v^2+p\\ (E+p)v\end{bmatrix}=0,\quad p=(\gamma-1)\cdot\left[E-\frac{\rho}{2}(u^2+v^2)\right].$$

The problem is initiated with a Mach 10 oblique shock positioned at (1/6, 0) which makes a 60° angel with $x$-axis. The computational domain is set to $[0,4]\times[0,1]$. The bottom boundary ($y=0$) consists of a reflecting wall beginning at $x=1/6$, and the short region from $x=0$ to $x=1/6$ is imposed with the initial post-shock conditions. The left boundary ($x=0$) is also assigned with the initial post-shock values, and at the right boundary ($x=4$), all the gradients are set to zero. The values along the top boundary ($y=1$) are set to describe the exact motion of the Mach 10 shock. We refer to [58] for more detailed descriptions. We compute the solution of density at $t=0.2$ with $480\times120$ mesh grids. Figure 10 shows the reference solution given by the fifth-order WENO finite difference method [45].

Figures 11 and 12 display the solutions computed with the NT scheme. It is clear from the results that the solution generated by the vA limiter has obviously better quality. The shock waves and the slip lines underneath are characterized by much sharper transitions. The computational results of the semi-discrete scheme are presented in Figs. 13 and 14. Still, the numerical scheme captures more information of the near-wall flow when used in conjunction with the vA limiter. These results confirm the advantage of the vA limiter (8) in terms of resolving multidimensional complex flow structures.

### 4.5 Incompressible Euler Equations

We consider the two-dimensional double shear layer problem for incompressible Euler equations

$$\begin{cases}\partial_t\mathbf{u}+\nabla\cdot(\mathbf{u}\otimes\mathbf{u})=-\nabla p,\\ \nabla\cdot\mathbf{u}=0,\end{cases}$$

where $p$ denotes the pressure and $\mathbf{u}=(u,v)$ is the velocity field. The initial data are given by

$$u(x,y,0)=\begin{cases}\tanh\left(\left(y-\frac{\pi}{2}\right)\Big/\rho\right), & y\leqslant\pi,\\ \tanh\left(\left(\frac{3\pi}{2}-y\right)\Big/\rho\right), & y>\pi,\end{cases}\qquad v(x,y,0)=\delta\sin(x)$$

over the rectangular domain $[0,2\pi]\times[0,2\pi]$. We take $\rho=\dfrac{\pi}{15}$ and $\delta=0.05$. The equations are solved with the finite difference projection method (see, e.g., [21, 31, 60]), which consists of a predictor step and a corrector step

$$\begin{aligned}&\frac{\mathbf{u}^*-\mathbf{u}^n}{\Delta t}+\nabla\cdot(\mathbf{u}^n\otimes\mathbf{u}^n)=0,\\ &\frac{\mathbf{u}^{n+1}-\mathbf{u}^*}{\Delta t}+\nabla p^{n+1}=0\quad\text{with}\quad\nabla\cdot\mathbf{u}^{n+1}=0.\end{aligned}$$

The divergence free constraint $\nabla\cdot\mathbf{u}^{n+1}=0$ leads to a Poisson equation for pressure

$$-\Delta p^{n+1}=-\frac{1}{\Delta t}\nabla\cdot\mathbf{u}^*.$$

In the predictor step, we reconstruct the convection fluxes $\mathbf{u}^n\otimes\mathbf{u}^n$ with the Rusanov-type flux (20) coupled with the second-order MUSCL reconstructions (17). In the corrector step, assuming the uniform mesh size is employed, $\Delta x=\Delta y=h$, the gradient, divergence, and Laplace operators are approximated with the second-order central difference operators

$$\begin{aligned}\nabla^h\phi_{i,j}&=\begin{pmatrix}\dfrac{\phi_{i+1,j}-\phi_{i-1,j}}{2\Delta x}\\ \dfrac{\phi_{i,j+1}-\phi_{i,j+1}}{2\Delta y}\end{pmatrix},\\ \nabla^h\cdot\mathbf{u}_{i,j}&=\frac{u_{i+1,j}-u_{i-1,j}}{2\Delta x}+\frac{v_{i+1,j}-v_{i-1,j}}{2\Delta y},\quad\mathbf{u}=(u,v),\\ \Delta^h\phi_{i,j}&=\frac{\phi_{i+2,j}-2\phi_{i,j}+\phi_{i-2,j}}{4\Delta x^2}+\frac{\phi_{i,j+2}-2\phi_{i,j}+\phi_{i,j-2}}{4\Delta y^2}.\end{aligned}$$

To achieve a higher order of accuracy in time, we apply the explicit SSPRK3 method for time marching. The time step is taken according to the CFL condition

$$\Delta t\max_{i,j}\left(\frac{|u_{i,j}|}{\Delta x}+\frac{|v_{i,j}|}{\Delta y}\right)\leqslant 0.5.$$

Figure 15 presents the solutions of vorticity at $t=8$. We observe that the solution contours given by the vA limiter are more concentrated than those by the minmod limiter. Figure 16 compares the solutions of $v$ along the line $x=\pi$. The vA limiter shows clear advantage over the minmod limiter in terms of capturing sharp extrema.

### 4.6 Concluding Remarks

The vA limiter dates back to the 1982 work [1]. Its TVD stability and related non-oscillatory properties were overshadowed by extensive studies of the class of minmod limiters [5,

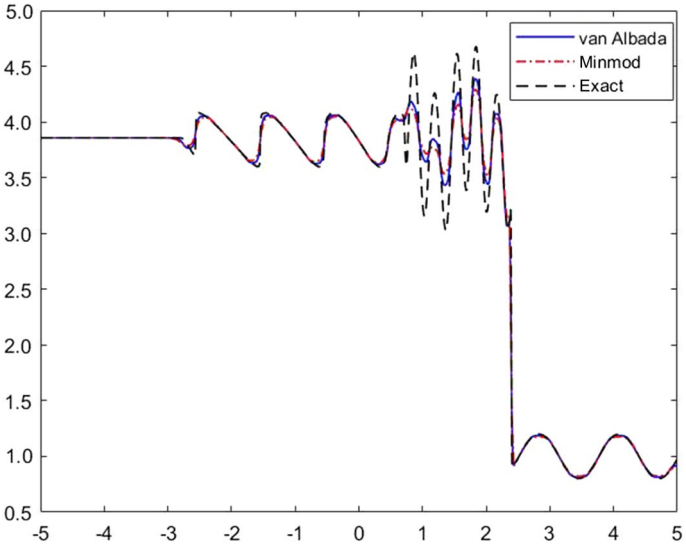


**Fig. 8** Osher-Shu problem—density, NT scheme, $N = 600$, $t = 1.8$

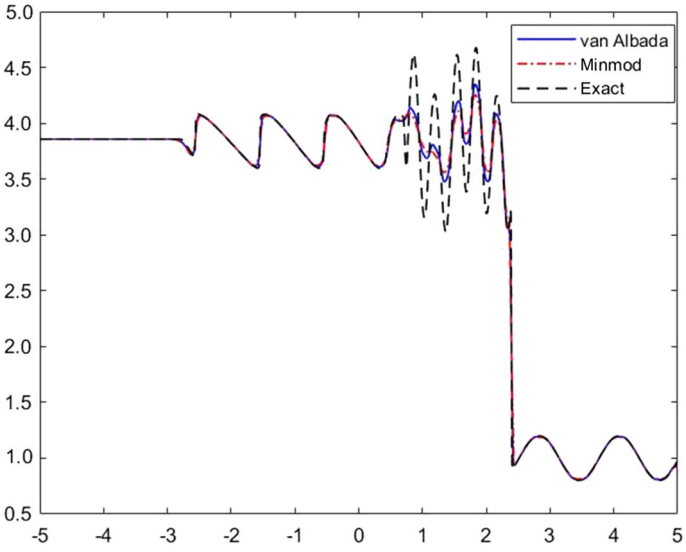


**Fig. 9** Osher-Shu problem—density, semi-discrete central-upwind scheme, $N = 600$, $t = 1.8$

14, 26, 27, 36, 39, 49]. In this work, we revisit the vA limiter in the context of high-resolution central schemes, showing that its non-oscillatory properties improve corresponding computations using the minmod limiter, or are at least on par with the minmod-based results in other computations. This was demonstrated in the one-dimensional Osher-Shu

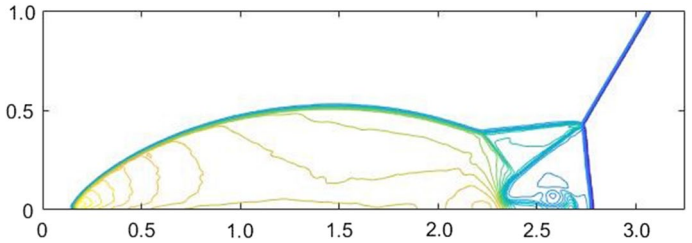


**Fig. 10** Double Mach reflection density, fifth-order WENO, $N_x = 480$, $N_y = 120$, $t = 0.2$

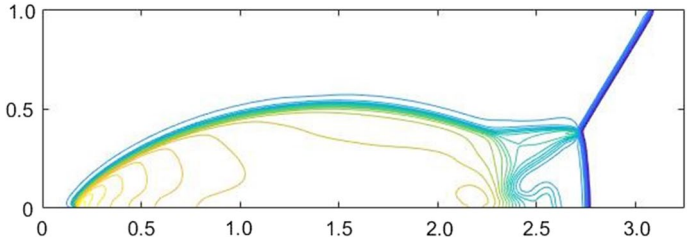


**Fig. 11** Double Mach reflection density, NT scheme, minmod limiter, $N_x = 480$, $N_y = 120$, $t = 0.2$

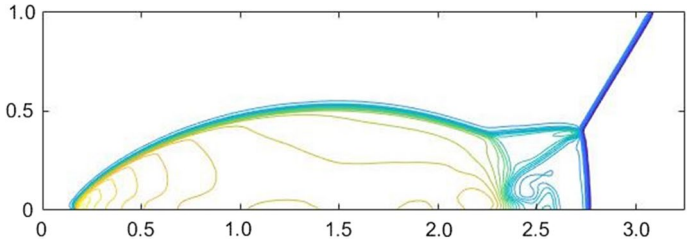


**Fig. 12** Double Mach reflection density, NT scheme, vA limiter, $N_x = 480$, $N_y = 120$, $t = 0.2$

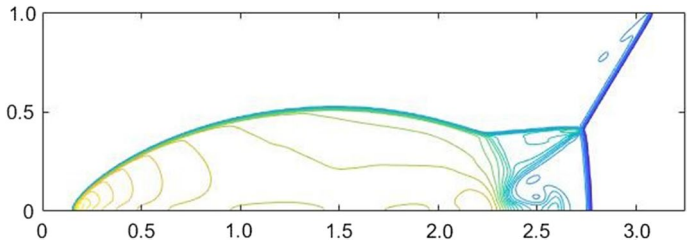


**Fig. 13** Double Mach reflection density, semi-discrete central-upwind scheme, minmod limiter, $N_x = 480$, $N_y = 120$, $t = 0.2$

problem depicted in Figs. 8 and 9 and more noticeably, in the two-dimensional problems reported in Sects. 4.4 and 4.5. We do not claim that the use of the vA limiter always outperforms the class of minmod limiters: the vA limiter is found on par with the minmod

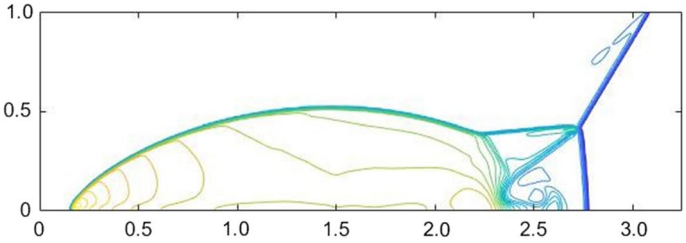


**Fig. 14** Double Mach reflection density, semi-discrete central-upwind scheme, vA limiter, $N_x = 480$, $N_y = 120$, $t = 0.2$

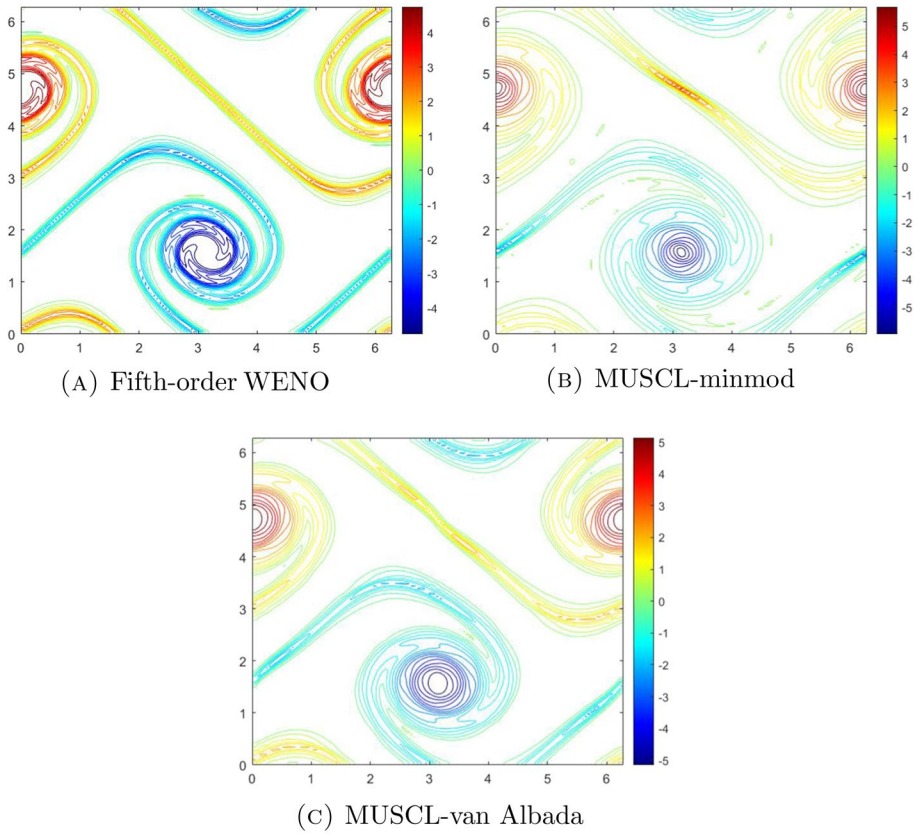


**Fig. 15** Double shear layer, contours of vorticity. $N_x = N_y = 128$, CFL $= 0.5$, $t = 8$

results for the one-dimensional Sod problem reported in Figs. 6 and 7; indeed, this is further highlighted in Fig. 17, where we zoom on the density variation of the Sod problem and observe comparable results for the vA limiter which is compared with the less diffusive minmod$_\theta$ with $\theta = \frac{1}{2}(1 + \sqrt{2})$ (corresponding to the upper bound on the right of (25a)). The main point here is to shed light on the smoother vA limiter, showing that it produces

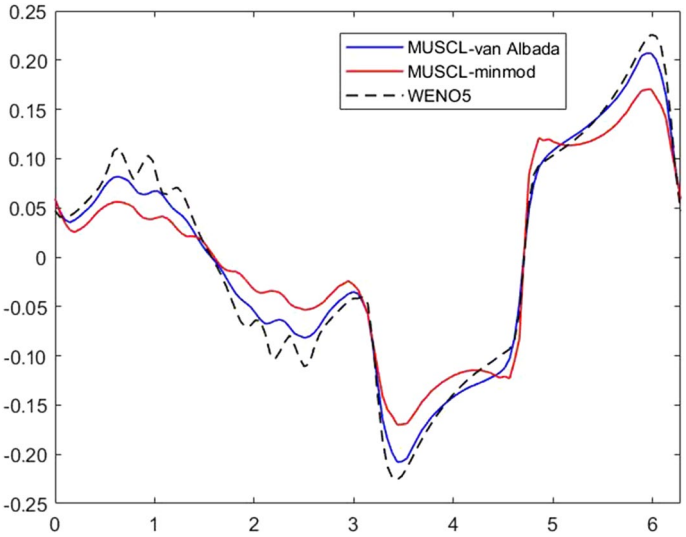


**Fig. 16** Double shear layer, solutions of $v$ along $x = \pi$, $N_x = N_y = 128$, CFL $= 0.5$, $t = 8$

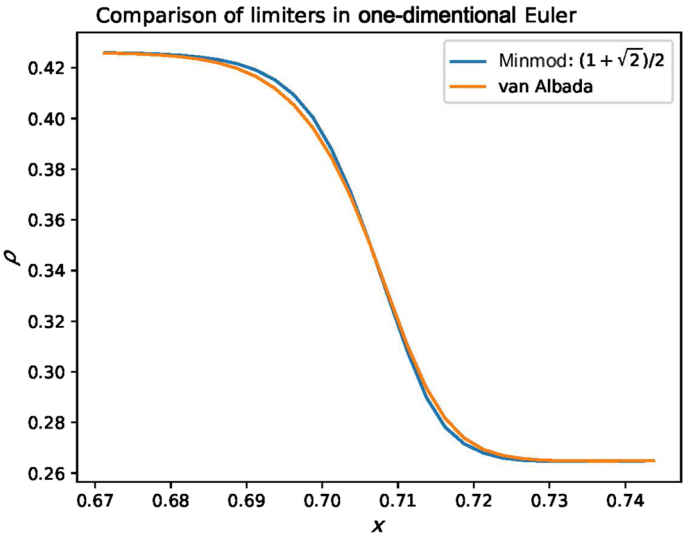


**Fig. 17** Sod's problem. Zoom on density computed by NT scheme, $N = 400$ at $t = 0.2$ using vA limiter vs. minmod$_\theta$ limiter with $\theta = 1.2$

equal or even better results than the class of minmod limiters. The vA limiter was added to the minmod limiter in the Python code [59] (solver scheme "sd3").

**Acknowledgements** Research was supported in part by the ONR Grant N00014-2112773.

## Compliance with Ethical Standards

**Conflict of Interest** On behalf of all authors, the corresponding author states that this work is in compliance with Ethical Standards, that we did not participate in any Research involving Humans/and or Animals under Compliance with Ethical standards, and that there is no conflict of interest.

## References


1. van Albada, G.D., van Leer, B., Roberts, W.W., Jr.: A comparative study of computational methods in cosmic gas dynamics. Astron. Astrophys. **108**(1), 76–84 (1982)
2. Arminjon, P., St-Cyr, A., Madrane, A.: New two- and three-dimensional non-oscillatory central finite volume methods on staggered Cartesian grids. Appl. Numer. Math. **40**(3), 367–390 (2002)
3. Balbás, J., Tadmor, E.: Central station—a collection of references on high-resolution non-oscillatory central schemes (2006). https://www.math.umd.edu/~tadmor/centpack/publications/
4. Balbás, J., Tadmor, E., Wu, C.-C.: Non-oscillatory central schemes for one- and two-dimensional MHD equations: I. J. Comput. Phys. **201**(1), 261–285 (2004)
5. Chakravarthy, S., Osher, S.: A new class of high accuracy TVD schemes for hyperbolic conservation laws. In: 23rd Aerospace Sciences Meeting, p. 363 (1985)
6. Einfeldt, B.: On Godunov-type methods for gas dynamics. SIAM J. Numer. Anal. **25**(2), 294–318 (1988)
7. Engquist, B., Osher, S.: One-sided difference approximations for nonlinear conservation laws. Math. Comput. **36**(154), 321–351 (1981)
8. Fjordholm, U.S., Mishra, S., Tadmor, E.: Arbitrarily high-order accurate entropy stable essentially nonoscillatory schemes for systems of conservation laws. SIAM J. Numer. Anal. **50**(2), 544–573 (2012)
9. Fjordholm, U.S., Mishra, S., Tadmor, E.: ENO reconstruction and ENO interpolation are stable. Found. Comput. Math. **13**, 139–159 (2013)
10. Fjordholm, U.S., Ray, D.: A sign preserving WENO reconstruction method. J. Sci. Comput. **68**, 42–63 (2016)
11. Godunov, S.K.: A finite difference method for the numerical computation of discontinuous solutions of the equations of fluid dynamics. Mat. Sb. **47**, 357–393 (1959)
12. Gottlieb, S., Ketcheson, D.I., Shu, C.-W.: Strong Stability Preserving Runge-Kutta and Multistep Time Discretizations. World Scientific, Singapore (2011)
13. Gottlieb, S., Shu, C.-W., Tadmor, E.: Strong stability-preserving high-order time discretization methods. SIAM Rev. **43**(1), 89–112 (2001)
14. Harten, A.: High resolution schemes for hyperbolic conservation laws. J. Comput. Phys. **135**(2), 260–278 (1997)
15. Harten, A., Engquist, B., Osher, S., Chakravarthy, S.R.: Uniformly high order accurate essentially non-oscillatory schemes, III. J. Comput. Phys. **71**(2), 231–303 (1987)
16. Harten, A., Hyman, J.M., Lax, P.D., Keyfitz, B.: On finite-difference approximations and entropy conditions for shocks. Commun. Pure Appl. Math. **29**(3), 297–322 (1976)
17. Harten, A., Lax, P.D., van Leer, B.: On upstream differencing and Godunov-type schemes for hyperbolic conservation laws. SIAM Rev. **25**(1), 35–61 (1983)
18. Harten, A., Osher, S.: Uniformly high-order accurate nonoscillatory schemes. I. In: Upwind and High-Resolution Schemes, pp. 187–217. Springer, Berlin (1997)
19. Jiang, G.-S., Tadmor, E.: Nonoscillatory central schemes for multidimensional hyperbolic conservation laws. SIAM J. Sci. Comput. **19**(6), 1892–1917 (1998)
20. Johnson, C., Szepessy, A., Hansbo, P.: On the convergence of shock-capturing streamline diffusion finite element methods for hyperbolic conservation laws. Math. Comput. **54**(189), 107–129 (1990)
21. Kupferman, R., Tadmor, E.: A fast, high resolution, second-order central scheme for incompressible flows. Proc. Natl. Acad. Sci. **94**(10), 4848–4852 (1997)
22. Kurganov, A., Levy, D.: A third-order semidiscrete central scheme for conservation laws and convection-diffusion equations. SIAM J. Sci. Comput. **22**(4), 1461–1488 (2000)
23. Kurganov, A., Noelle, S., Petrova, G.: Semidiscrete central-upwind schemes for hyperbolic conservation laws and Hamilton-Jacobi equations. SIAM J. Sci. Comput. **23**(3), 707–740 (2001)
24. Kurganov, A., Tadmor, E.: New high-resolution central schemes for nonlinear conservation laws and convection-diffusion equations. J. Comput. Phys. **160**(1), 241–282 (2000)

25. Lax, P.D.: Weak solutions of nonlinear hyperbolic equations and their numerical computation. Commun. Pure Appl. Math. **7**, 159–193 (1954)
26. van Leer, B.: Towards the ultimate conservative difference scheme. V. A second-order sequel to Godunov's method. J. Comput. Phys. **32**(1), 101–136 (1979)
27. van Leer, B.: On the relation between the upwind-differencing schemes of Godunov, Engquist-Osher and Roe. SIAM J. Sci. Stat. Comput. **5**(1), 1–20 (1984)
28. Levy, D., Puppo, G., Russo, G.: Central WENO schemes for hyperbolic systems of conservation laws. ESAIM Math. Model. Numer. Anal. **33**(3), 547–571 (1999)
29. Levy, D., Puppo, G., Russo, G.: A third order central WENO scheme for 2D conservation laws. Appl. Numer. Math. **33**(1/2/3/4), 415–421 (2000)
30. Levy, D., Puppo, G., Russo, G.: A fourth-order central WENO scheme for multidimensional hyperbolic systems of conservation laws. SIAM J. Sci. Comput. **24**(2), 480–506 (2002)
31. Levy, D., Tadmor, E.: Non-oscillatory central schemes for the incompressible 2-D Euler equations. Math. Res. Lett. **4**(3), 321–340 (1997)
32. Liu, X.-D., Osher, S., Chan, T.: Weighted essentially non-oscillatory schemes. J. Comput. Phys. **115**(1), 200–212 (1994)
33. Liu, X.-D., Tadmor, E.: Third order nonoscillatory central scheme for hyperbolic conservation laws. Numer. Math. **79**(3), 397–425 (1998)
34. Liu, Y., Shu, C.-W., Tadmor, E., Zhang, M.: $L^2$ stability analysis of the central discontinuous Galerkin method and a comparison between the central and regular discontinuous Galerkin methods. ESAIM Math. Model. Numer. Anal. **42**(4), 593–607 (2008)
35. Mulder, W.A., van Leer, B.: Experiments with implicit upwind methods for the Euler equations. J. Comput. Phys. **59**(2), 232–246 (1985)
36. Nessyahu, H., Tadmor, E.: Non-oscillatory central differencing for hyperbolic conservation laws. J. Comput. Phys. **87**(2), 408–463 (1990)
37. Osher, S.: Riemann solvers, the entropy condition, and difference. SIAM J. Numer. Anal. **21**(2), 217–235 (1984)
38. Osher, S.: Convergence of generalized MUSCL schemes. SIAM J. Numer. Anal. **22**(5), 947–961 (1985)
39. Osher, S., Tadmor, E.: On the convergence of difference approximations to scalar conservation laws. Math. Comput. **50**(181), 19–51 (1988)
40. Piperno, S., Depeyre, S.: Criteria for the design of limiters yielding efficient high resolution TVD schemes. Comput. Fluids **27**(2), 183–197 (1998)
41. Roe, P.L.: Approximate Riemann solvers, parameter vectors, and difference schemes. J. Comput. Phys. **43**(2), 357–372 (1981)
42. Saurel, R., Abgrall, R.: A simple method for compressible multifluid flows. SIAM J. Sci. Comput. **21**(3), 1115–1145 (1999)
43. Shu, C.-W.: TVB uniformly high-order schemes for conservation laws. Math. Comput. **49**(179), 105–121 (1987)
44. Shu, C.-W.: Total-variation-diminishing time discretizations. SIAM J. Sci. Stat. Comput. **9**(6), 1073–1084 (1988)
45. Shu, C.-W.: Essentially non-oscillatory and weighted essentially non-oscillatory schemes for hyperbolic conservation laws. In: Cockburn, B., Shu, C.-W., Johnson, C., Tadmor, E. (eds.) Advanced Numerical Approximation of Nonlinear Hyperbolic Equations, pp. 285–372. Springer, Berlin (1998)
46. Shu, C.-W.: Essentially non-oscillatory and weighted essentially non-oscillatory schemes. Acta Numer. **29**, 701–762 (2020)
47. Shur, M.L., Spalart, P.R., Strelets, M.K.: Noise prediction for increasingly complex jets. Part I: methods and tests. Int. J. Aeroacoust. **4**(3), 213–245 (2005)
48. Spiteri, R.J., Ruuth, S.J.: A new class of optimal high-order strong-stability-preserving time discretization methods. SIAM J. Numer. Anal. **40**(2), 469–491 (2002)
49. Sweby, P.K.: High resolution schemes using flux limiters for hyperbolic conservation laws. SIAM J. Numer. Anal. **21**(5), 995–1011 (1984)
50. Tadmor, E.: Numerical viscosity and the entropy condition for conservative difference schemes. Math. Comput. **43**(168), 369–381 (1984)
51. Tadmor, E.: Convenient total variation diminishing conditions for nonlinear difference schemes. SIAM J. Numer. Anal. **25**(5), 1002–1014 (1988)
52. Tadmor, E.: Total variation and error estimates for spectral viscosity approximations. Math. Comput. **60**(201), 245–256 (1993)

53. Tadmor, E.: Approximate solutions of nonlinear conservation laws and related equations. In: Cockburn, B., Shu, C.-W., Johnson, C., Tadmor, E. (eds.) Advanced Numerical Approximation of Nonlinear Hyperbolic Equations, pp. 1–149. Springer, Berlin (1998)
54. Tadmor, E.: Entropy stability theory for difference approximations of nonlinear conservation laws and related time-dependent problems. Acta Numer. **12**, 451–512 (2003)
55. Tadmor, E.: Selected topics in approximate solutions of nonlinear conservation laws. High-resolution central schemes. In: Nonlinear Conservation Laws and Applications, pp. 101–122. Springer, New York (2011)
56. Toro, E.F., Spruce, M., Speares, W.: Restoration of the contact surface in the HLL-Riemann solver. Shock Waves **4**(1), 25–34 (1994)
57. Wang, S., Xu, Z.: Total variation bounded flux limiters for high order finite difference schemes solving one-dimensional scalar conservation laws. Math. Comput. **88**(316), 691–716 (2019)
58. Woodward, P., Colella, P.: The numerical simulation of two-dimensional fluid flow with strong shocks. J. Comput. Phys. **54**(1), 115–173 (1984)
59. Zenginoglu, A.: Centpy: central schemes for conservation laws in python (2020). https://pypi.org/project/centpy/
60. Zhang, J., Jackson, T.L.: A high-order incompressible flow solver with WENO. J. Comput. Phys. **228**(7), 2426–2442 (2009)